Graduate School of Frontier Sciences, The University of Tokyo
Department of Socio-Cultural Environmental Studies

2022

Master's Thesis

Mangrove Extent and Species Distribution in the Fukido River Estuary, Ishigaki Island

石垣島吹通川河口域におけるマングローブ林の面積と種の分布解析

Submitted on July 15, 2022

Advisor: Professor Jun SASAKI

Phyo Thet Naing

ピョ テットナイング

47-206805

ABSTRACT

The mangrove ecosystem is a potential sink of atmospheric carbon dioxide for the global carbon cycle and provides essential services for the coastal communities for living, shelter, and food as well as sediment trapping and coastal defense from natural disasters. Even though mangroves provide such valuable services to coastal dwellers, mangrove forests are the world's most threatened habitat due to other land-use changes such as infrastructure development, aquaculture expansion, salt, and rice production within mangrove areas, as well as human settlement within mangrove areas. The causes of the expansion or regression of mangrove forests are the effects of anthropogenic factors such as sea level rising and climate change, which result in global warming and sedimentation increasing along the coastal regions. Consequently, these factors have been threatening the existence of mangrove forests and the distribution of species because of sedimentation and tidal inundation changes. For that reason, conserving the remaining mangrove forests are one of the crucial issues for future mangrove conservation. In general, mangrove forests are located in inaccessible areas. Therefore, remote sensing technique plays an important role for monitoring the mangrove forests such as assessing the mangrove distribution, and species level mapping. Some studies have attempted to extract the mangrove distribution using satellite imagery, and hyperspectral imagery with different classification methods, but there is limited information using drone imagery with convolutional neural network (CNN) based on texture extraction for mangrove classification. Moreover, some researchers pointed out that using deep neural networks to detect mangrove forests from remote sensing imagery shows the best performance of semantic segmentation in image processing. In this study, the U-Net model under CNN-based classification was therefore applied for the classification of the mangrove distribution with drone imagery under the complex land cover in order to propose texture extraction-based classification for the mangrove distribution. Species-level classification was also extracted using Random Forest (RF) and discussed the species distribution changes in the Fukido river mangrove areas by integrating field observation data. In the present investigation, the U-Net model under Convolutional Neural Network was first applied for mangrove distribution using drone imagery with texture information. Based on the results of hyper-parameter tuning, the

performance of the model achieved for mangrove distribution with an overall accuracy of 95.70%. In addition, this study provided that the current mangrove tree-distributed area in the Fukido river estuary was 15.05 ha. Furthermore, the creation of ground truth data based on the iterative self-organizing data analysis algorithm (ISODATA) used by this study could be helpful information to assist in creating the ground truth (label) data for the other mangrove scattered regions. Secondly, this study implemented mangrove species level classification with Random Forest in the Fukido river estuary. The result of species level classification showed that the overall accuracy was 82.7 %. According to the results of the species-level classification, the *Bruguiera gymnorhiza (B.gymnorhiza)* was dominantly distributed over the study area, while the *Rhizophora stylosa (R. stylosa)* was dominant not only along the creek (river) but also in some high ground areas. Finally, the species distribution changes were studied based on field observation data. As a result, some parts of *R.stylosa* could survive under the competition with *B.gymnorhiza* in the *B.gymnorhiza*-dominated area by increasing the tree height. Moreover, according to the results of the relative tide inundation duration (RID), there was no significant relationship between the distribution of species and the tidal inundation in this study because some parts of *R.stylosa* could survive at high ground level. Based on the research findings, this study shows that the U-Net model using drone imagery supports good performance for the classification of mangrove distribution under complex land cover and discusses the distribution of species changes by integrating with field observation data in the Fukido river estuary.

ACKNOWLEDGEMENT

First and foremost, I would like to express my heartfelt thanks to my respected supervisor, Professor Jun SASAKI, for his acceptance as a master's student in his laboratory at the great and honorable university, "The University of Tokyo", and for his valuable guidance during my master's journey that instructed me "how to approach research", and explanation and teaching me very details, even in the training of drone driving and others. I could not express my gratitude to my professor with words for his patience and valuable time.

Secondly, I also deeply thank my co-supervisor, Professor Hiroyasu SATOH, for his kind guidance, and helpful suggestions and advice for the preparation of my master's thesis and presentation as well.

Thirdly, my special gratitude extends to the Forest Department, Ministry of Natural Resources and Environmental Conservation, Myanmar for giving me a chance to study abroad and supporting everything throughout my master's life.

I am grateful to Win Sithu Maung, who is a doctoral student at the University of Tokyo, Hongo campus, for his encouragement and support to upgrade my academic profile at UTokyo for my future career. In addition, I also want to express my most profound gratitude to Nagamura Wataru, who is a doctoral student, for his support during the field trip and data analysis, and Dr. Chen Jundong, from Professor Jun Sasaki's Lab in the Department of Socio-cultural Environment Studies, for helping me with machine learning.

I would like to express my deepest thanks to the Asian Development Bank (ADB)-Japan Scholarship Program (ADB-JSP scholarship program) for supporting my studies and giving me a chance to taste the higher education system of Japan. Additionally, I am extremely thankful to Ms. Mari Matsuoka, who is a representative officer for the ADB scholarship program (International Liaison Office) for her patience and support at every stage of academic life in Japan while attending at UTokyo.

Last but not least, I would be remiss in not mentioning my family for the emotional support and other things during this study.

TABLE OF CONTENTS

LIST OF FIGURES

LIST OF TABLES

Chapter 1 INTRODUCTION

1.1. Background Information

Mangrove forests can be found between approximately 30° North and 30° South in the tropical and subtropical regions of the world as the inter-tidal areas between the land and the sea [1]. The distribution of mangrove forests is from the mean sea level to the highest spring tide [2]. They provide coastal communities with services such as timber and fuel wood, fisheries, sediment trapping and coastal defense from disasters, and carbon storage that can store 3-4 times more carbon than other upland forests [3]. The mangrove ecosystem is a potential sink of atmospheric carbon dioxide for the global carbon cycle [4], and it stores a lot of carbon not only in its soil but also in aboveground and belowground biomass as well as in dead organic substances. In addition, mangroves also support maintaining the water quality of coastal regions and provide a beneficial ecosystem for the coral reefs and seagrass beds [5].

Even though mangroves provide a lot of service to coastal dwellers, mangrove forests have been the most threatened habitat overall in the world [6]. Furthermore, all the remaining mangrove forests could disappear in the next 100 years if the rate of continuous mangrove degradation is not stopped [7]. The main drivers for mangrove degradation and deforestation are other land-use changes including infrastructure development, aquaculture expansion, salt, and rice production in mangrove areas, as well as urban development, especially in Asia-Pacific regions [8]. Furthermore, many regions around the world have faced such challenges to the expansion or regression of mangroves as a result of anthropogenic factors such as sea level rise and climate change, resulting in global warming and increased sedimentation along coastal regions [9]. Moreover, Gilman et al. [10] also pointed out that rising sea level is also one of the greatest drivers of mangrove loss.

Nowadays, many donor organizations and local governments have been trying to restore and rehabilitate the mangrove forests by using different kinds of approaches to recover the mangrove loss because of its plenty of support for disaster prevention and climate change mitigation. Besides, conserving the remaining mangrove forests are also one of the crucial issues in the aspect of mangrove conservation. In general, the

distribution of mangrove forests is in inaccessible areas. Therefore, remote sensing technique plays an important role for monitoring the mangrove forests such as assessing the mangrove distribution, and species level mapping.

Giri et al. [11] produced the first mangrove map using over 1000 Landsat scenes with automatic and manual classification techniques applying remote sensing data, dating from 1997 and 2000. After that, some studies have analyzed the mangrove extent detection and mapping of species distribution using free satellite data such as Landsat and Sentinel satellites, and aerial imagery (drone, hyperspectral drone) with different classification methods for global and local level analysis based on their research purposes.

In the case of Japan's mangroves, Japan’s mangrove forests are an important source for supporting coastal fisheries [12]. Over the past decades, the cause of mangrove loss in Japan was the overexploitation of timber and tannin production [13], but the utilization of timber or tannin has already been banned in Japan. Furthermore, mangrove loss has increased due to anthropogenic factors such as urban development, road construction, and industrial development [14]. Moreover, in the coastal regions of Okinawa prefecture, there was very high sedimentation increasing along the coast because of a poor land-use management system that was threatening the existence of mangrove areas in some places [15]. Additionally, the improvement of ecotourism services such as speed boats driving around the mangrove areas could lead to harm to the mangrove forests in some areas as well [16].

The Ministry of the Environment in Japan has already laid out the distribution of mangrove areas around Japan as a reference map for mangrove conservation. For Japan’s regional level mangrove map, Bayan et al. extracted the distribution of mangrove forests map for Kyushu, Tanega, Amami-O, Okinawa, Ishigaki, and Iriomote Islands by integrating the spectral analysis of Landsat Enhanced Thematic Mapper Plus (ETM+) with a Digital Elevation Model (DEM) at a regional scale [17]. The distribution of mangrove forests in Ishigaki Island was 87 ha (using Landsat satellite image), 80 ha using Sentinel image (Baloloy et al. 2021), and 100 ha (Ministry of Environment Reference Map) respectively.

The study area, Fukido River Mangrove Park, was protected as a national sanctuary according to the Ministry of the Environment of Japan [18]. The mangrove area of the Fukido river is approximately 20.04 ha according to Baloloy et al. 2021, who developed the estimation of mangrove distribution areas using the mangrove vegetation index (MVI) that comes from Sentinel satellite images and mapped the zonation of species distribution for that area [19]. However, mapping accuracy is dependent on the methods and the datasets of input features. Mapping with satellite imagery provides global and regional level maps for mangrove species distribution, but the resolution of the satellite is coarser than that of unmanned aerial vehicles (drones). As a result, the estimation of mangrove extent is different [20]. For these reasons, the ability of drones become useful for mangrove extent mapping because of their fine resolution. In addition, sea level rising and extreme weather conditions such as storms could threaten the balance between salt and fresh water [21]. Consequently, these factors could affect the distribution of mangrove species changes because of sedimentation and tidal inundation changes. The previous studies in the Fukido river regions for mangrove distribution and species zonation mapping were based on satellite imagery with traditional machine learning approaches. Despite such kinds of information existing in the Fukido river mangrove area, there is a gap in information to analyze the distribution of mangrove extent and species-level classification by drone imagery with deep learning and the cause of species distribution changes by integrating with field observation for more accurate monitoring and sustainable mangrove management for the future.

1.2. Objectives of the study

The overall objective is to study the mangrove extent and species distribution changes in the Fukido river estuary using drone imagery, and field observation data. In order to achieve the overall objective, three main specific objectives of this study were identified as below.

i. To extract the mangrove distribution area using texture information with a Convolutional Neutral Network (CNN)
ii. To analyze the species level distribution based on tree canopy structure using Random Forest (RF)
iii. To discuss the current situation of species distribution changes

1.3. Literature review

1.3.1. Mangrove Extent Mapping with Convolutional Neural Network

Remote sensing plays an important role in monitoring the mangrove forests, such as mangrove distribution and species level mapping, and aboveground biomass estimation as well [22-23]. Some studies have attempted to extract the mangrove distribution using different satellite images with Random Forest (RF), Support Vector Machine (SVM), Artificial Neutral Network (ANN), and Convolution Neural Network (CNN).

A few studies have used mangrove classification using deep learning because it is a bit difficult to construct a dataset. The development of semantic segmentation is to extract objects from images for pixel-level classification [24]. Due to the current development of Convolutional Neural Networks (CNN) [25-26], the performance of semantic segmentation has been significantly enhanced because of deep feature extraction from downsampling [27-28]. For deep learning approaches, CNNs have been widely used for image recognition [29–30], and the extraction of information from an image [31–32] because of the advantages of data processing power and learning capacities.

For CNN-based mangrove classification, Yichao et al. developed GC-UNet that improved upon the U-Net model for mangrove segmentation using Landsat 8 imagery [33]. Furthermore, Sentinel-2 and Worldview 2 imagery were used to map mangrove distribution on a large scale in Fiji using a deep convolutional neural network [34]. ME-Net was also created by Guo et al. using Sentinel-2A imagery for mangrove extraction [35].

Moreover, some researchers pointed out that using deep neural networks to detect mangrove forests from remote sensing imagery shows the best performance of semantic segmentation in image processing [36-40]. Therefore, the U-Net model under CNN-based classification was applied using high-resolution drone imagery for the extraction of the mangrove area in this study.

1.3.2. Mangrove species mapping

Mangrove species level mapping is one of the big challenges than mangrove mapping using remote sensing [41]. Some studies have used mangrove species classification using various microwave datasets [42]. In addition, Pham et al. used a logistics tree model classifier using ALOS-2 microwave data for two mangrove species classifications [43]. Cao et al. also used unmanned aerial vehicles (UAVs), hyperspectral images, and digital surface models (DSMs) with object-based classification to classify mangrove species [44].

Additionally, the classification of three mangrove species was also conducted using a multi-sensor dataset with Random Forest by Arasumani et al. [45]. Naidoo et al. implemented the savanna species classification using the Random Forest Model by integrating hyperspectral and LiDAR measurements [46]. Furthermore, Behera et al. studied the mangrove species level classification and mapping a mangrove forest using AVIRIS-NG and Sentinel data with the Random Forest model [47]. Most of the studies used satellite images, hyperspectral imagers, and lidar data for mangrove species mapping with different classification methods such as logistic tree model classifier, random forest model, and object-based classification. But there is no information for drone imagery classification with random forest for mangrove species level classification according to the literature review. Therefore, this study focused on the mangrove species level classification with drone imagery using a random forest model.

1.4. Study Significance

According to the literature review, the present study is the first effort to extract mangrove extent using a Convolutional Neural Network (U-Net) using drone (rgb images) because most of the studies for mangrove extent extraction were using free satellite images, commercial satellite images, and Hyperspectral Drone images, and Drone RGB with digital elevation model for mangrove distribution with different classification methods, such as RF, SVM, ROF, ANN, CNNs with different parameters. In this study, the distribution of mangrove forests was extracted using drone-based texture extraction applying deep learning under the situation of complex land cover.

In addition, in this study, ground truth data creation was carried out with the assistance of the iterative self-organizing data analysis algorithm (ISODATA) and then self-classified the accrual mangrove distribution extent based on field survey and the texture information of the orthomosaic. Hence, the creation of ground truth data based on ISODATA used by this study could be helpful information to assist in creating the ground truth (label) data for the other mangrove scattered regions. Additionally, this study provided that the current mangrove tree-distributed area in the Fukido river estuary for future sustainable mangrove monitoring and management. Moreover, an abnormal pattern of species distribution was also observed based on the field observation data. As a result, this study contributed not only to the mangrove extent mapping using drone imagery with a deep learning model but also to abnormal species distribution, which was also discussed by integrating with field observation data.

Chapter 2 MATERIALS AND METHODS

2.1. Study Area

The study area, the Fukido river estuary, is located between 24° 27' 0" and 24° 30' 0" North and 124° 13' 37.2" and 124° 14' 9.6" East on Ishigaki Island, Okinawa Prefecture, the southwestern part of Japan (Figure 2.1). The Fukido river mangrove is renowned for "Fukidogawa River Mangrove Colony" (Iriomote-Ishigaki National Park) and the surrounding areas include some residential areas, mountainous areas, paddy fields, and the open sea. The annual mean temperature and precipitation of the Fukido river regions were 24°C and 2095 mm, respectively, up to the year 2020, based on the data of the Japan Meteorological Agency. The mangrove species in this area are typically dominated by true mangrove species, namely: *Bruguiera gymnorrhiza* **(***B.gymnorrhiza***)** and *Rhizophora stylosa (R.stylosa)***.**

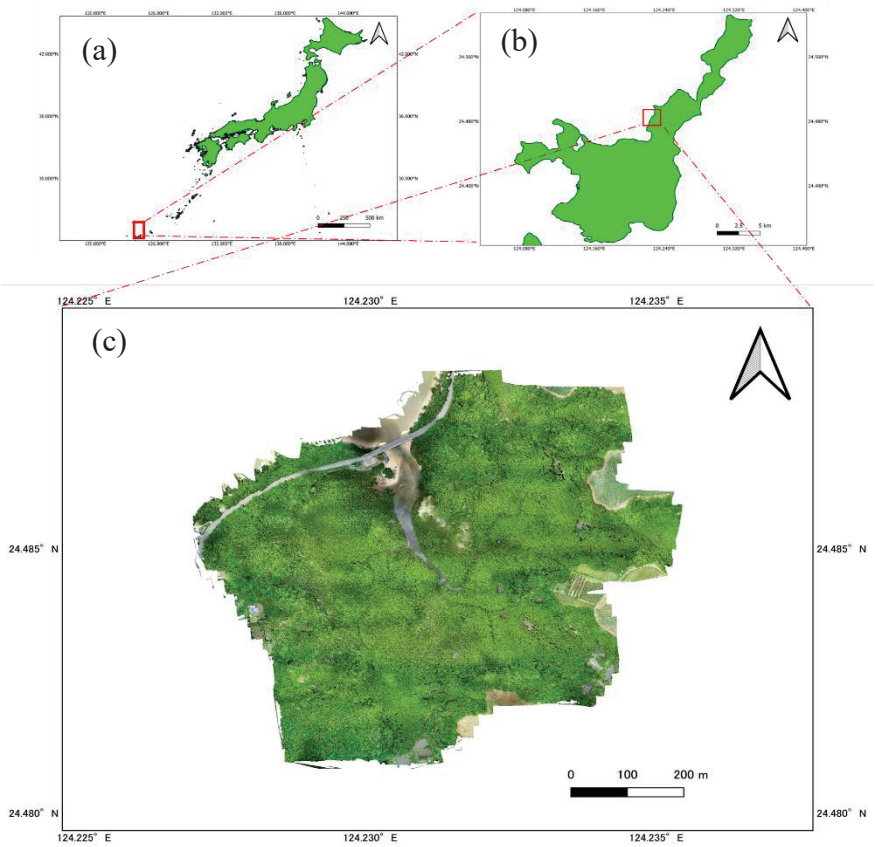

Figure 2.1 Location of the study area (a) Japan, (b) Ishigaki Island, (c) fukido river (orthomosaic)

2.2. Field Observation

2.2.1. Drone Images Acquisition

The aerial imagery was taken using Phantom 4 Pro V2 (SZ DJI TECHNOLOGY CO., LTD.) (Figure 2.2) with red-green-blue (RGB) sensor on 15th and 16th August 2021. In addition, DJI GS Pro (Ground Station Pro) software is an open-source application for controlling and planning automatic flights for DJI aircraft. Therefore, DJI Ground Station Pro software (Figure 2.3) was used for controlling and planning flight tracks at 80-meter (m) altitude for the entire mangrove areas and 30 m altitude for some areas above ground level with 90 % front and 80 % side overlap, a flight speed of 4 ms^{-1} during a survey. The reason why 80 m and 30 m altitudes were applied for drone photogrammetry in this study is that most of the previous studies used 120 m, and 100 m altitudes for mangrove and/ or species mapping because of the large mangrove extent and based on their research purpose. However, the coverage photo of this study is 34.25 Hectares (ha), and the size of mangrove trees in some areas is a bit smaller than in the other areas. Therefore, 80 m altitude for the entire mangrove forest was used in this study. Table 2.1 describes the specific parameters for the planning of flight tracks using DJI GS Pro software.

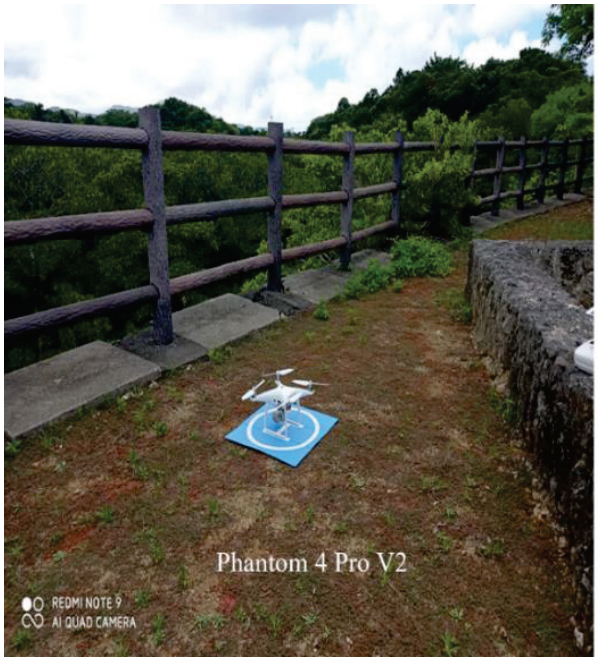

Figure 2.2 (a) Phantom 4 Pro V2 (Drone), (b) DJI GS Pro software

Table 2.1 describes the specific parameters for the planning of flight tracks using DJI GS Pro software.

Particular	Parameters
Camera Model	Phantom 4 Pro V2 Camera
Shooting Angle	Parallel to Main Path
Capture Mode	Capture at Equal Distance Interval
Flight Course Mode	Scan Mode
Speed	4.0 M/S
Height	80.0M/ 30.0 M
Resolution	2.2 CM/ PX. 4.0 CM/ PX
Front Overlap Ratio	90 %
Side Overlap Ratio	80 %
Gimble Pitch Angle	-90%
End Mission Action	Return to Home

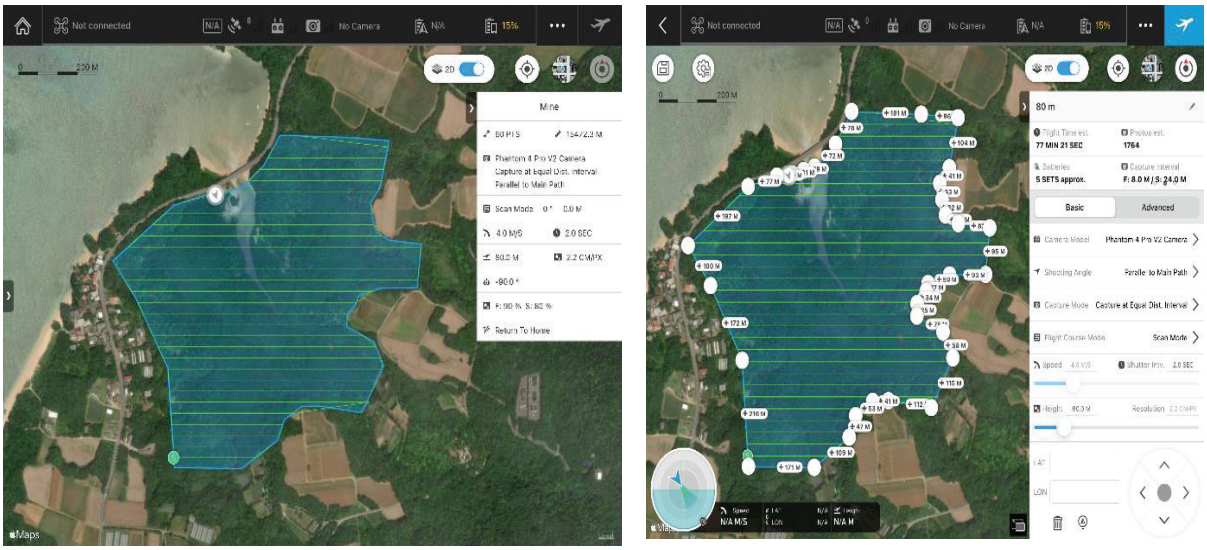

Figure 2.3 Setting up the details parameters for drone flying using DJI GS Pro software

2.2.2. Tree data collection

Field observation for the whole area was performed to inspect mangrove extent and species distribution before deciding on the field sample plots. The collection of tree data was conducted from August 23rd to September 2nd, 2021. Only two mangrove species were observed in this study area. The location of sample plots was decided based on the tree species distribution patterns and abnormalities that mean *R. stlyosa* species are competing with the other species of *B.gymnorhiza.* For collecting the tree data information, 10 m circular plot was created to check the distribution of species at random. Figure 2.4 illustrates the plot design for the collection of tree data in this study. The design of a circular plot is very easy to create in the field and is an efficient way to measure the tree height and diameter at breast height (DBH) (Figure 2.5) [48]. The reason for creating a 10 m plot is to obtain more species diversity within the plots. Within the circular plot, the location of the central point was first defined to divide into four parts that could easily collect the data and reduce the overlapping of sample data. After establishing the circular plot, tree height and diameter at breast (DBH) data were recorded using a height measurement pole for tree height (Figure 2.6), and a clipper for DBH measurement. The total number of sample plots was 9 in this study, and the location of each plot and the number of trees that were collected from field observation were described in Appendix 1.

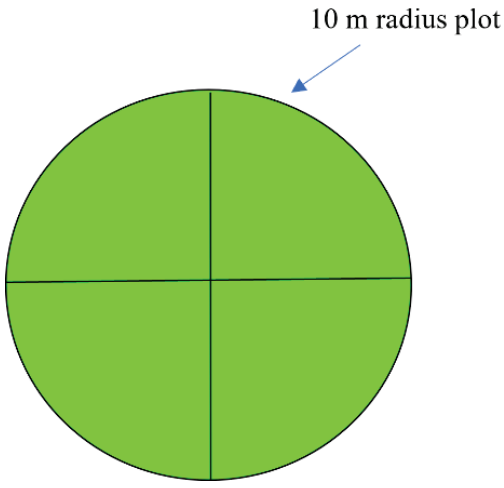

Figure 2.4 10 meters radius plot for collecting tree data information such as height and diameter at breast height (DBH)

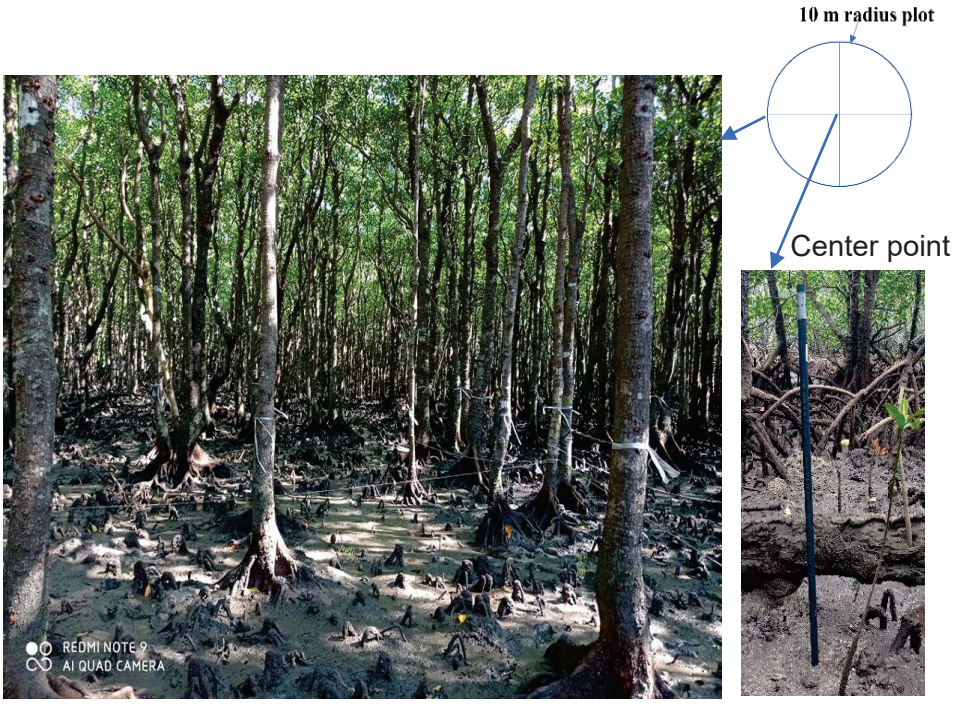

Figure 2.5 Selecting center point and recorded the tree data within the 10 m radius plot

Figure 2.6 The measurement of Tree Height within the plot using pole

2.2.3. Water level data collection

The collection of water level data was implemented from August 23rd to September 2nd, 2021, to discuss the distribution of species with tidal inundation. The two HOBO water level loggers (LGR S/N: 20936273 and 20796938) were set up in the plot locations to analyze tide level changes from the base station to the plots (Figure 2.7). The water level loggers provided information on water pressure, temperature, and atmospheric pressure, which were measured from the field with 0.10% full-scale accuracy with 4, 9, and 30-meter resolution to collect water level. The base station of the HOBO device was in front of the mangrove forests, and the other two water level loggers were set up two days per plot in line with the tree data collection plots. The water level was calculated using the following equation 2, derived from equation 1. The location of each plot is described in Appendix 2.

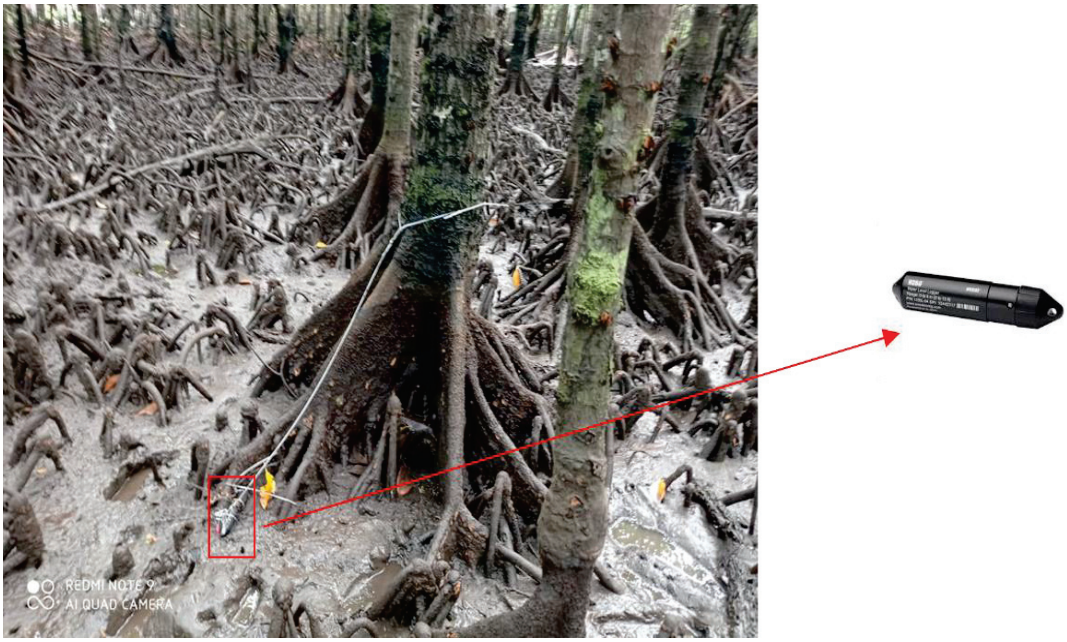

Figure 2.7 Setting up the water level logger (HOBO onset) inside the plots

$$P = \rho gh \quad (1)$$

$$h = \frac{(P_{air} - P_{water})}{\rho g} \quad (2)$$

where,

P = Pressure in water and air (Pa)

ρ= water density (g/cm^3)

g = gravitational acceleration (m/s^2)

h = water level height (m)

2.2.4. Calculation of Tide Inundation data

After calculating the water level data for the base station and 9 plots, the duration of tide inundation was calculated using the following equation (3). The water level data at the base station is very important to calculate the difference between the base station and plots to get relative inundation (RID) data. The value of RID from the plots is equal to 100%, which means the level of ground height is nearly the same as the base station. Moreover, the RID value is equal to zero, showing no mangrove exists in these areas, which means land forested or other land use. The detailed calculation is described in Figure 2.8.

$$RID = \frac{\text{Inundation duration at a Plot}}{\text{The time of Water level change at the Base}} \text{ x } 100 \quad -------- (3)$$

where,

RID = Relative Inundation Duration (%)

Water level change at the Base station = minutes

Inundation Duration at a Plot (minutes) = Swamp inundation time at one tide cycle

Calculating tidal cycle from water level data for the base station and the plots (for example, base station and plot number 3)

- Red point shows the beginning and the end of one tidal cycle
- The tide inundation for every tidal cycle within two days between the base station and the plots was calculated for tide duration, and then, the average and standard deviation of the total tide inundation were used for calculation.

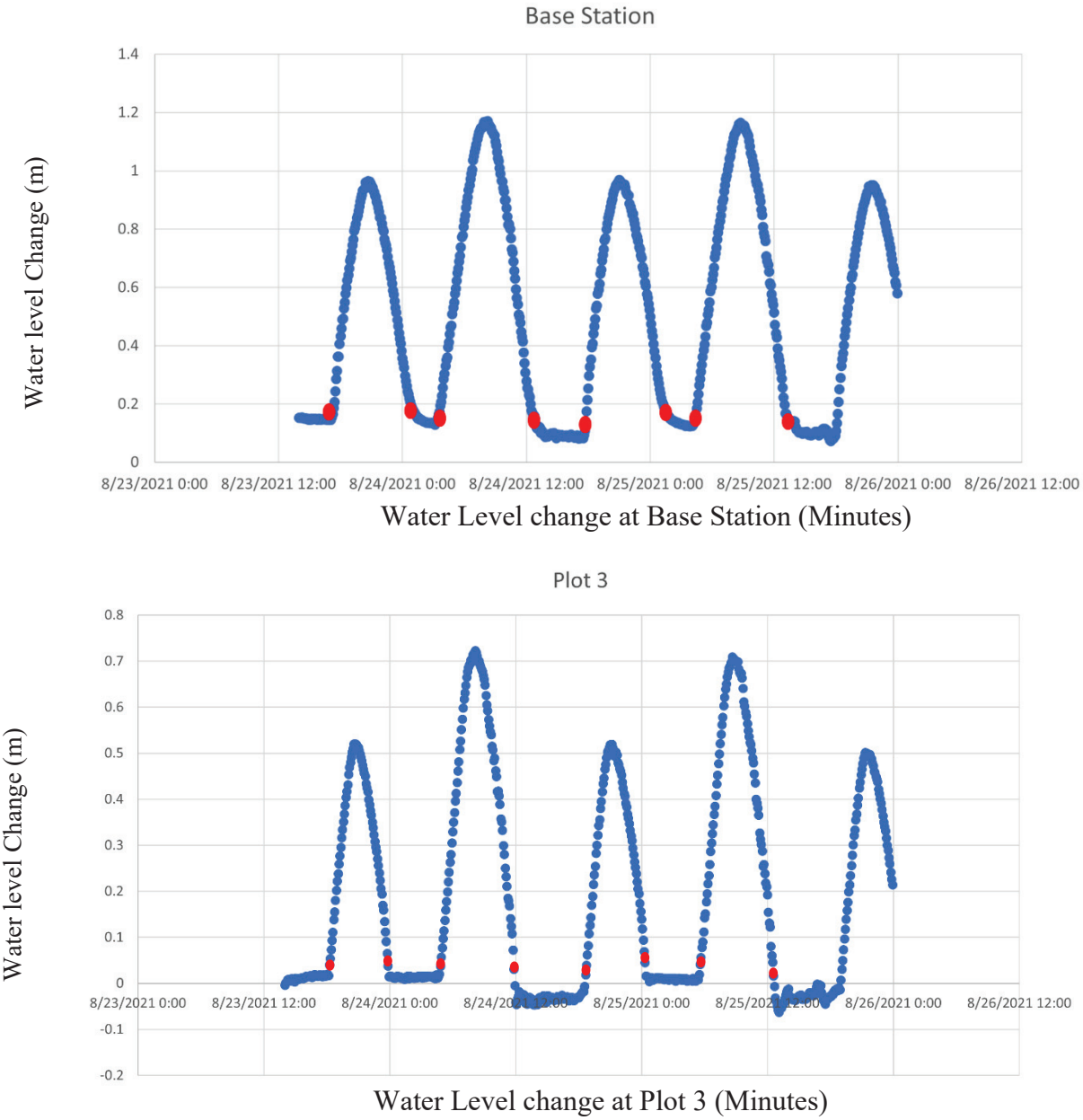

Figure 2.8 Calculating Relative Inundation Duration from the data of base and plots water level data

2.3. Creation of Datasets for Classification

2.3.1. Drone Image Processing

The processing of the aerial imagery was conducted using Agisoft Metashape Professional, which is software for performing digital image processing and generating 3D spatial data for GIS applications. Three main steps needed for image processing in this software are: (1) image alignment based on the features of the images, which depends on the position of the camera; (2) generating 3D surface models and Digital Elevation Models (DEM) based on dense point clouds from camera positions; and (3) building georeferenced Orthomosaic dependent on the DEM or mesh data. The processing steps contain the following details:

1. Loading images into Metashape;
2. Checking loaded images, and removing overlapped images (unnecessary images)
3. Aligning the photos (cameras)
4. Building dense point cloud
5. Building 3D polygonal model
6. Generating texture
7. Building tiled model
8. Building digital elevation model (DEM)
9. Building orthomosaic
10. Exporting results

The total number of photos that were taken by drone at 80 m altitude was 2,051 photos. All the photos were added to the Agisoft Metashape professional software for image processing. Figure 2.9 and Table 2.2 describe the general workflow and processing time of photogrammetry.

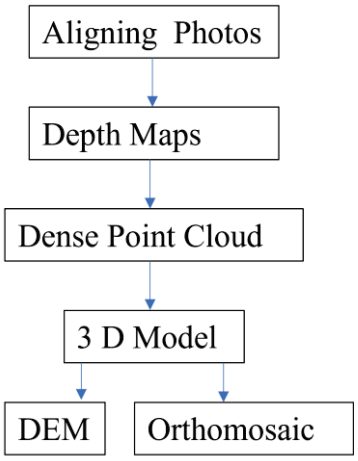

Figure 2.9 The general workflow of Drone Image Processing

Table 2.2 shows the processing time for photogrammetry using high performance computer

Steps	**Details**	**Processing Time**
Aligning Photos		
Depth Maps	Depth maps generation parameters	13 hrs 14 minutes
Dense Point Cloud	Dense cloud generation parameters	1 day 18 hours
3 D Model	-Reconstruction parameters -Texturing parameters	20 minutes 3 seconds 1 hour 48 minutes
DEM	Reconstruction parameters	3 minutes 8 second
Orthomosaic	Reconstruction parametes	2 hours 6 minutes

*Processing time will be different based on the performance of the computer

DEM = Digital Elevation Model

Orthomasic = "an aerial photograph geometrically corrected ("orthorectified") such that the scale is uniform"

2.3.2. Tree Structure Information

Two main mangrove species that exist in the Fukido River estuary are called *R. stylosa* and *B. gynorrhiza.* The tree crown and root structure of the two species are different (Figure 2.10). The mangrove distribution and species mapping were based on the tree crown structure of these species. The crown color of *R.stylosa* is dark green when visually interpreted from the orthomosaic (Figure 2.11), and the crown pattern of this species has a lot of side branches rather than the *B.gymnorrhiza***,** which has a light green crown structure from the orthomosaic (Figure 2.12), and the crown shape is almost round.

(a) ***B. gymnorhiza*** (b) ***R. stylosa***

Figure 2.10 Tree structure of (a) B.gymnorhiza, (b) R.stylosa (side photo)

Figure 2.11 Tree crown shape of R.stylosa (captured from orthomosaic)

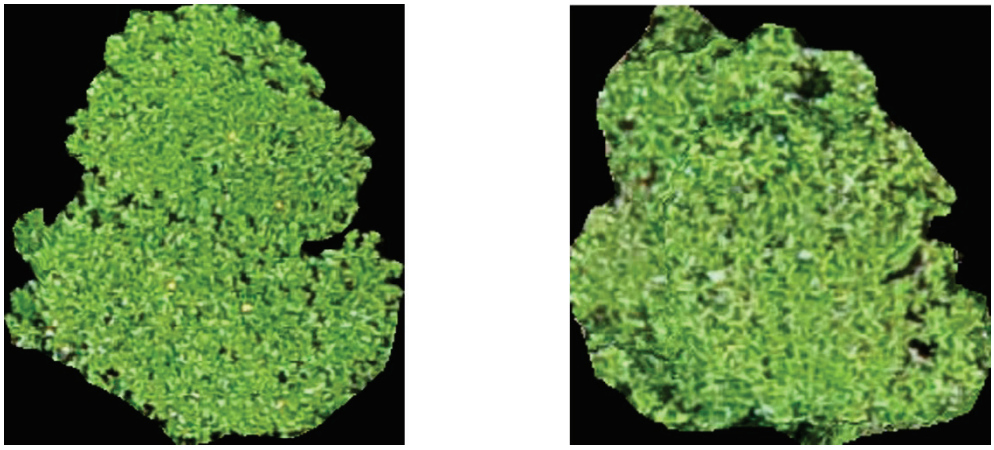

Figure 2.12 Tree crown shape of the B.gymnorrhiza (captured from Orthomosaic)

2.3.3. Creation of Ground Truth data using ISO Unsupervised Classification for mangrove classification

The creation of ground truth data is a big challenge for supervised classification and deep learning in the remote sensing field. To attain more accurate ground truth data, the iterative self-organizing data analysis algorithm (ISODATA) in ArcGIS Pro 2.6.0 was used to assist in creating ground truth data for classification. According to the complex land cover of the study area, the mangrove and non-mangrove areas were manually extracted based on the DSM (height information), field observation data, and visual interpretation of the orthomosaic image, which means the mountain areas and actual mangrove distribution areas, before applying ISODATA.

To reduce missed classification and processing time, the original photo was divided into five parts (figure 2.13) which each of the split photos was classified using the ISODATA. The number of classes, minimum class size, and sampling interval for classification in the Iso cluster unsupervised classification is needed to set up for image classification. In this study, 30 classes size, a sampling interval of 10, and a minimum class size of 20 were used for classification, and then the classified output images were obtained with clusters of 30 categories. After getting the classified result, reclassification tools were used to assign two classes:

mangrove and non-mangrove. At this stage, self-identification for separating the two classes is needed, therefore, the mangrove areas and non-mangrove areas were assigned based on the structure of the mangrove trees and the other non-mangrove areas from the orthomosaic for visual interpretation. After applying the same process for the other part of the split photo, all the classified ground truth images were combined from different parts into the entire one for classification. The raster value 0 for non-mangrove and 255 for mangrove was obtained as a binary raster, and then, assigned the ground truth image with the same resolution of the orthomosaic for final classification. For example, the details of the explanation for the ground truth creation of the binary class were shown in Figures (2.14 to 2.17).

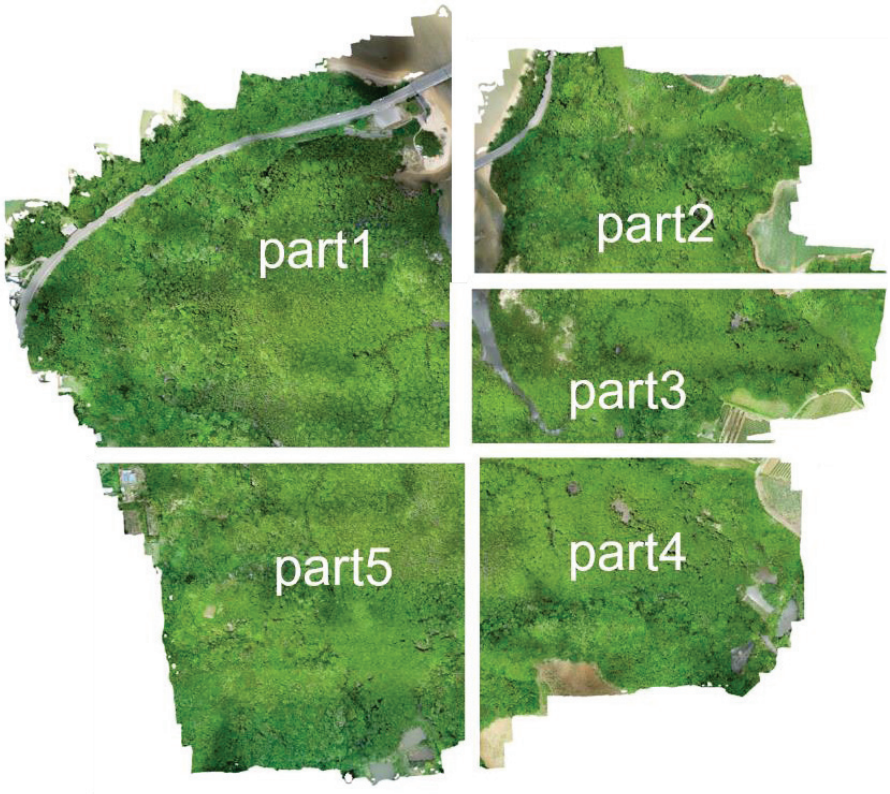

Figure 2.13 Dividing the orthomosaic photo to five parts for creating ground truth data

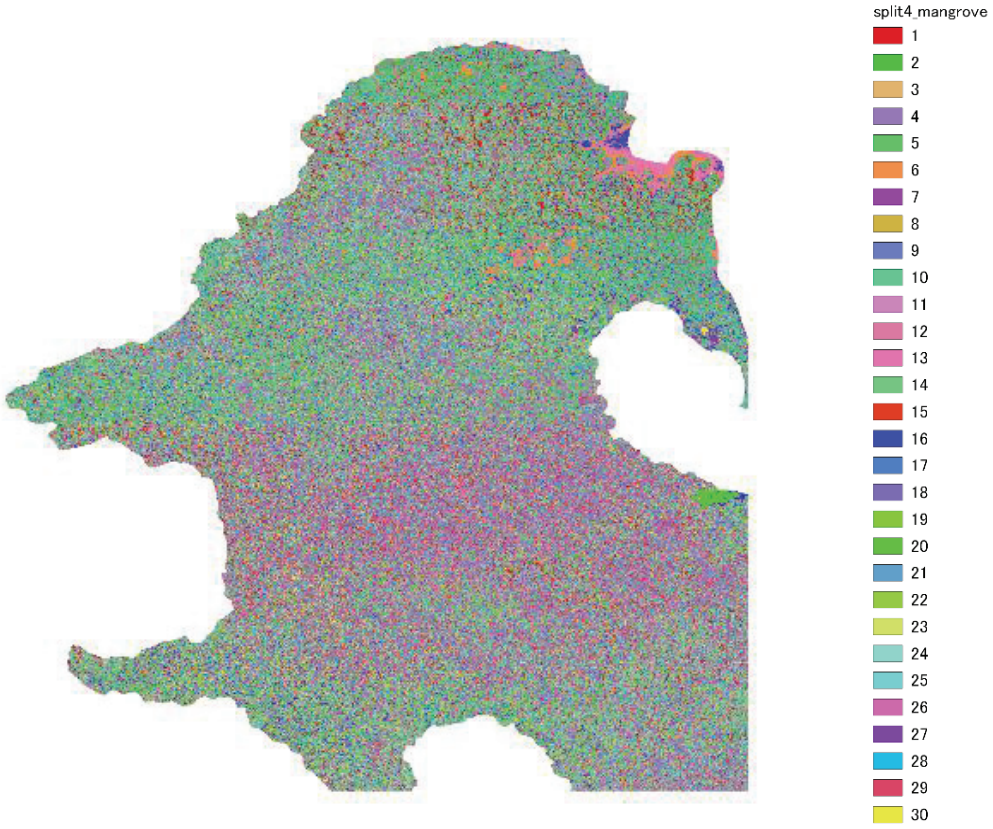

Figure 2.14 Appling iso supervised classification and self-identification

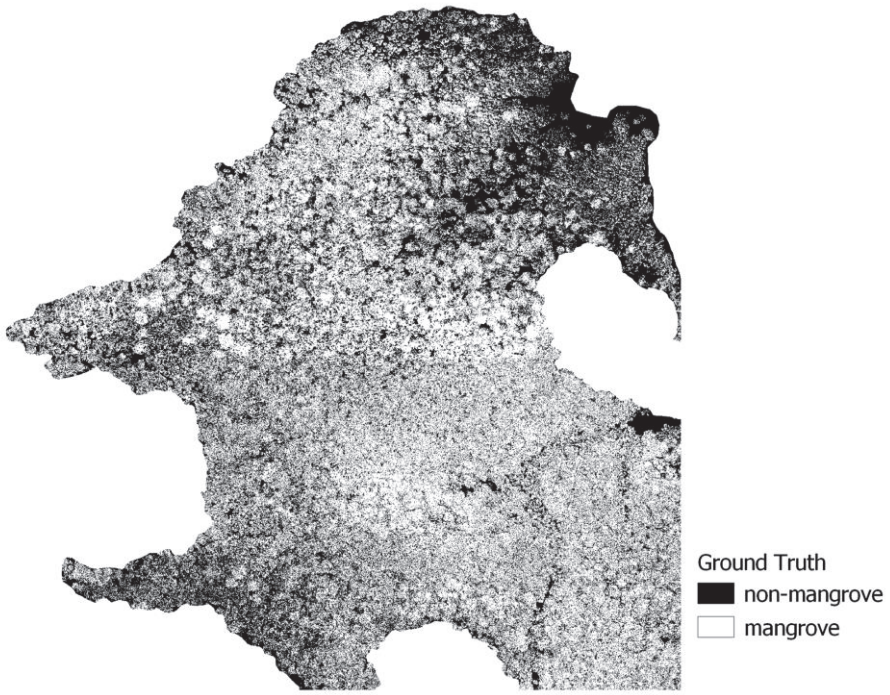

Figure 2.15 Reclassify the raster into mangrove and non-mangrove

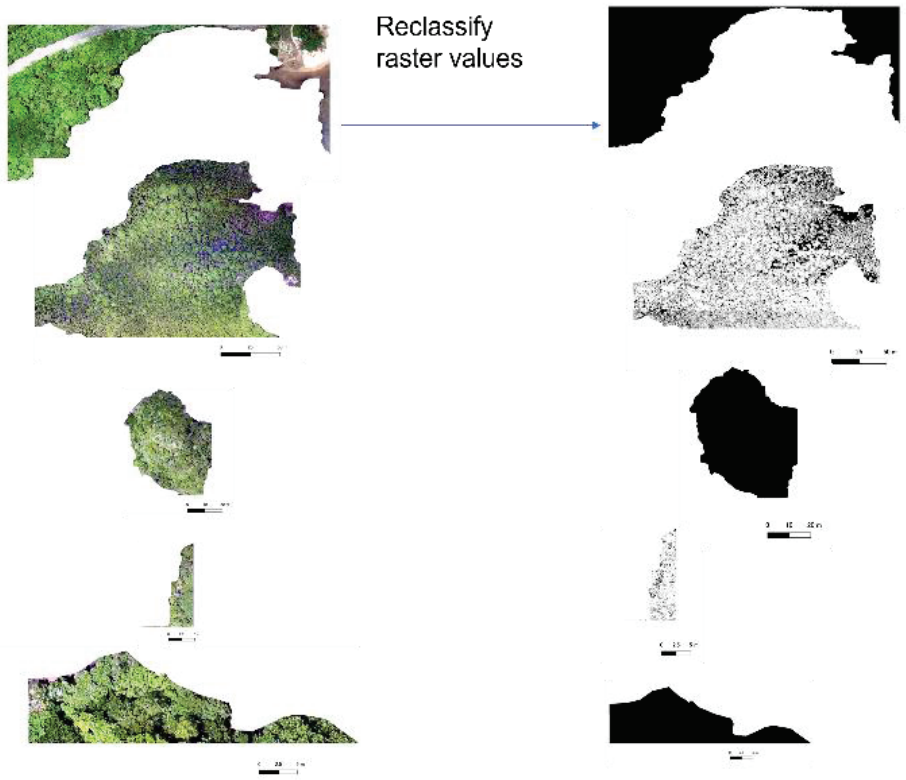

Figure 2.16 Detail procedures for ground truth data

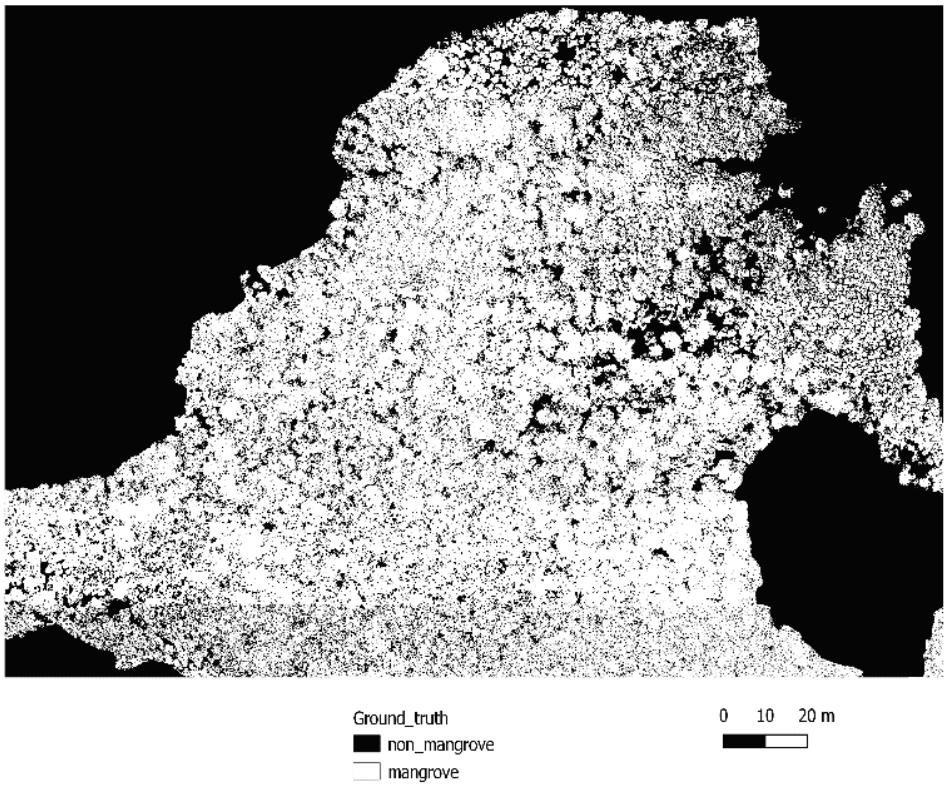

Figure 2.17 Final ground truth for mangrove classification (for example)

2.3.4. Creation of ground truth data for species level classification

The creation of the ground truth data for species-level classification was conducted based on the tree crown structure and color of the *R. stylosa* and *B. gymnorhiza* when visually interpreted from the orthomosaic (Figure 2.11, 2.12). Using the orthomosaic, polygons were manually drawn based on the tree crown structure in QGIS software. For species analysis, three main classes were assigned: R. stylosa, B. gymnorhiza, and land and water areas. After creating the polygon data, the assigned polygons were converted into raster in random forest classification. The detailed procedure for creating ground truth data for species classification was described in Figure 2.18.

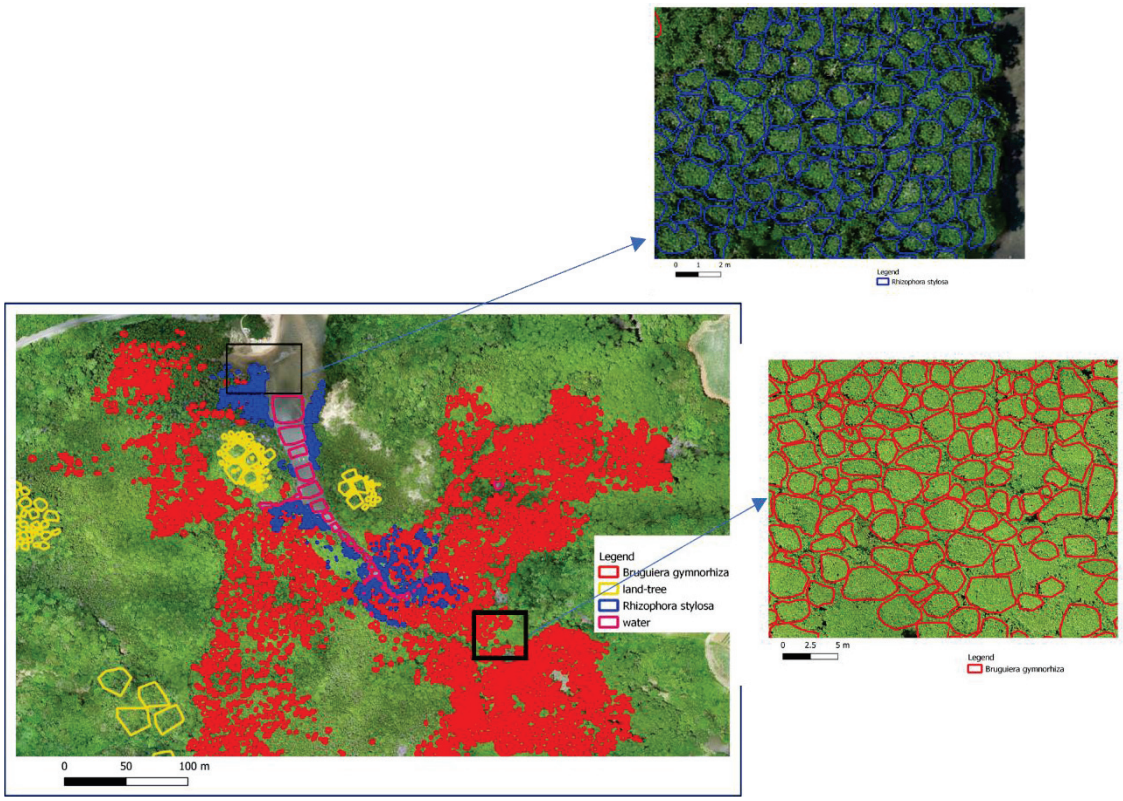

Figure 2.18 Detail procedures for creating ground truth data for species classification

2.4. Convolutional Neural Network for mangrove mapping

The U-Net architecture was designed for biomedical image segmentation by Ronneberger et al., 2021[49]. Nowadays, CNN is a popular deep learning method for image segmentation, objection detection. In addition, image segmentation is a kind of stage for computer vision to represent the different segmented images' parts for each different class of the image. The network of the UNet architecture consists of two parts: the first part was called a contraction path (so-called encoder path) on the left-hand side, and the second path was called the symmetric expanding path (called decoder) on the right-hand side of Figure 2.19. It consists of the repeated application of two 3 x 3 convolutions (unpadded convolutions) and a 2 x 2 max pooling operation with two strides for downsampling. The framework of the U-Net architecture was described as follows (Figure 2.19):

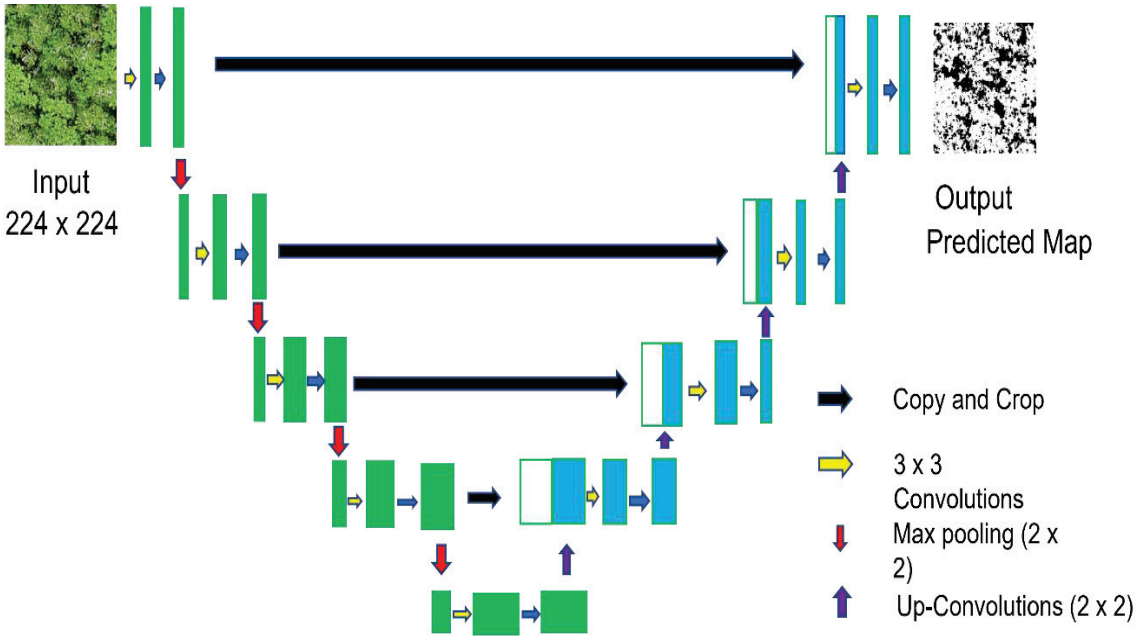

Figure 2.19 The Framework of The UNet model used in this study for image classification

2.4.1. The workflow, and input data preparation for experiment

The dataset of the input data (orthomosaic) and the ground image raster must have the same resolution (the same extent) for data argumentation (Figure 2.20). As a dataset preparation, 90% of the original image was assigned to the training part, and 10% of the photo to the testing part. The spatial resolution of the orthomosaic image used in this study is 0.03 m. The orthomosaic and ground truth data were clipped by a 224 x 224 randomly sliding window for training data classification. In addition, Pycharm Community Edition 2020.3 was used to perform the experiments with the deep learning toolkit Pytorch on NVIDIA GeForce RTX 2080 Ti and CUDA 11.0 on Windows 10. The input data for the training process was assigned to the training dataset (80%), the testing dataset (10%), and the validation dataset (10%) using the PyTorch dataset extractor. The model was then trained using the training dataset with 200 epochs for all the experiments to select the optimal overall accuracy through the model performance. The environmental setting for deep learning with PyTorch on Window system is shown in Appendix 3.

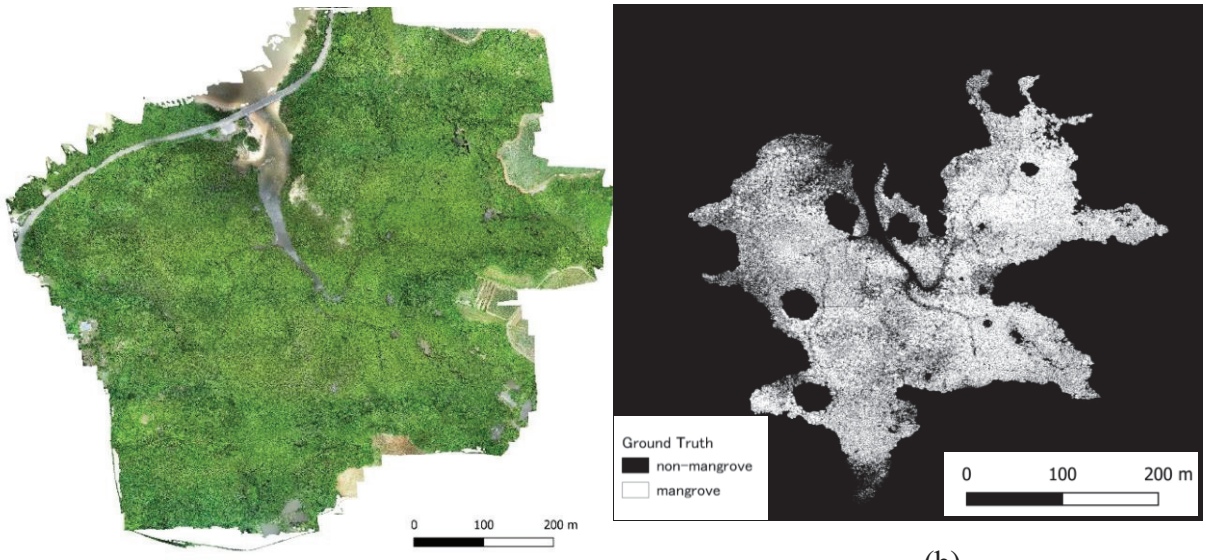

(a) (b)

Figure 2.20 The preparation of input data: (a) orthomosaic, (b) ground truth data

The workflow for mangrove mapping is described as Figure 2.21.

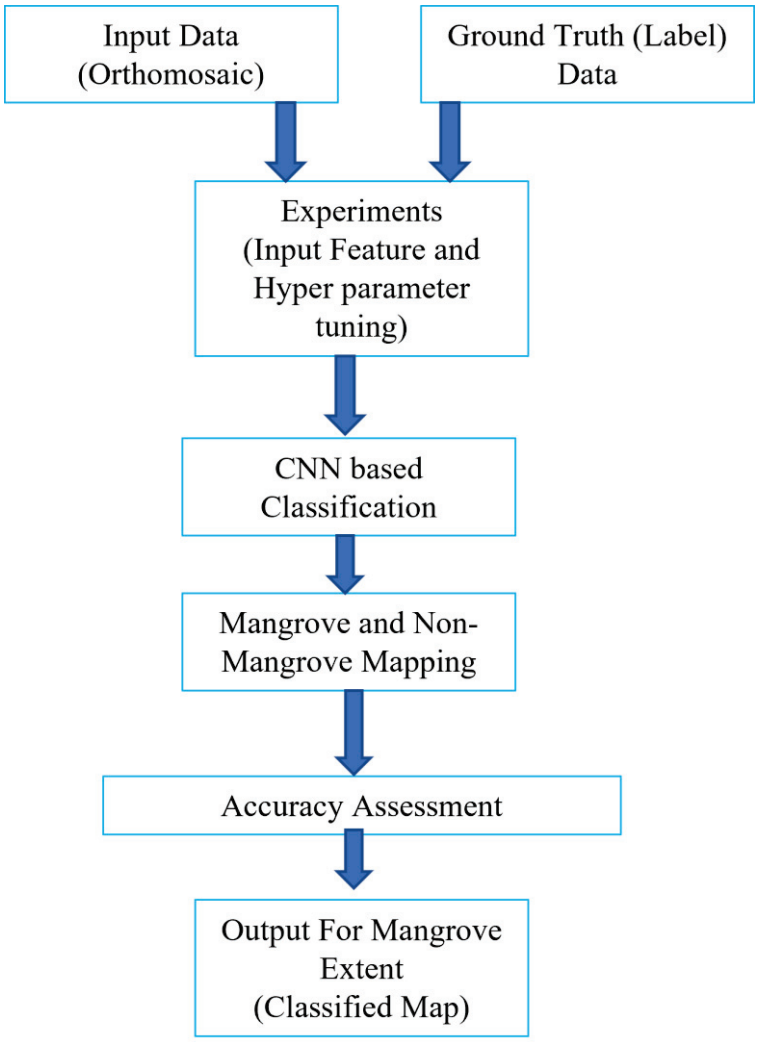

Figure 2.21 The Workflow of mangrove distribution using CNN

2.4.2. Hyper-parameter tunning for mangrove distribution

The hyperparameter tuning of this model was performed with the number of kernel sizes, the number of batch sizes, and the learning rate for training the model. The tuning of hyperparameters could improve the overall accuracy of the model. After getting a trained model, it could be applied to the testing dataset for accuracy assessment. Table 2.3 describes the experiments for hyperparameter tuning in the U-Net model.

Table 2.3. Hyper-parameter tunning in U-Net

Number	Learning Rate	Batch size	Number of base kernels
T1	0.0002	32	24
T2	0.0002	32	32
T3	0.0001	24	32
T4	0.0001	24	16
T5	0.0001	24	64
T6	0.001	16	32
T7	0.001	32	16

2.5. Species level mapping with Random Forest

The Random Forest (RF) classifier is a machine learning algorithm that applies multiple trees based on randomly selected sample data [50]. It is an ensemble method for classification trees, and each tree is supported with a single vote for the input data [51]. Furthermore, random forest builds many binary classification trees from the original observation using many bootstrap samples [52]. The samples that are left out from the bootstrap sample are called out-of-bag (OOB) samples [53]. The OOB sample data was used to evaluate the misclassification error rate and the estimate of the important variable. In addition, the performance of the random forest classifier was dependent on two parameters, such as the number of decision trees and the input variable [54]. A Random Forest classifier was used for species-level mapping using Python software in this study.

2.5.1. The workflow, and input data preparation for species classification

After mapping mangrove distributed areas, mangrove areas were extracted based on the classified image of mangrove distribution. The ground truth data for species-level classification was identified as a vector file (shape file) based on the structure of two species. As a dataset preparation, the ground truth data was split into 70% for training the model and 30% for the testing part, respectively. The workflow for species-level mapping is described the following Figure 2.22.

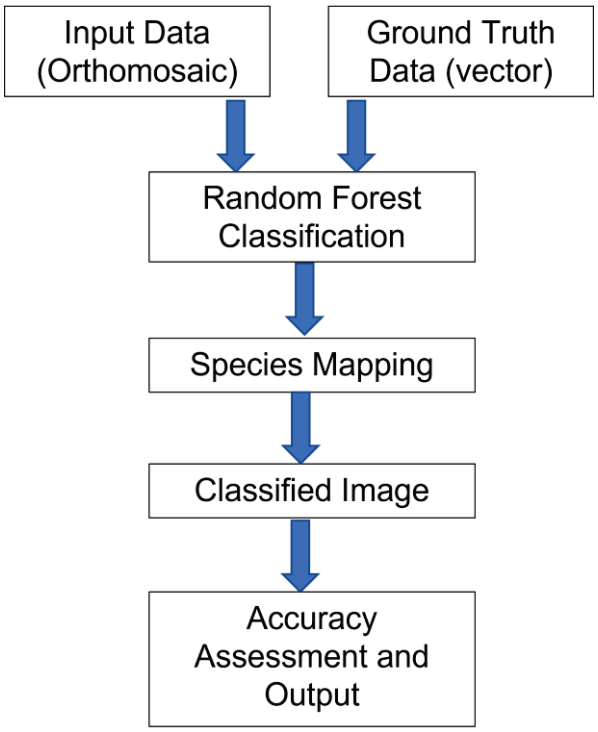

Figure 2.22 The Workflow of species level classification using Random Forest

2.6. Accuracy Assessment

The accuracy of the classified image is important to evaluate the performance of the model and the classification accuracy. The result of the trained models was changed into a confusion matrix or the matrix of error, which represents every pixel of the classified images. The classified images were defined into four categories, such as true positive (TP), false positive (FP), false negative (FN), and true negative (TN), compared with the data of the ground truth image. The value range is between 0 and 1, and the

classification results are close to 1, which is the highest accuracy of the classification. For assessing the evaluation of the classified images, the following five equations were used for accuracy assessment:

$$\text{Overall Accuracy} = \frac{TP+TN}{TP+TN+FP+FN} \quad ---------- (4)$$

$$\text{Precision} = \frac{TP}{TP+FP} \quad ----------(5)$$

$$\text{Recall} = \frac{TP}{TP+FN} \quad ----------(6)$$

$$\text{F1-score} = \frac{2 \times \text{Precision} \times \text{Recall}}{\text{Precision}+\text{Recall}} \quad ----------(7)$$

$$\text{Intersection over unio (IoU)} = \frac{TP}{TP+FP+FN} \quad ----------(8)$$

Chapter 3 RESULTS

3.1. Results from drone data processing

The results from drone data processing for the whole area at 80 m altitude, the ground resolution of the orthomosaic was 2.12 cm/pixel at 41,679 x 40,704 (Figure 3.1). In addition, the ground resolution of the Digital Surface Model (DSM) was 4.23 cm/pixel at 30,419 x 31,317 (Figure 3.2). The coverage of the orthomosaic was 34.25 hectares (ha), and the geographical coordinate system was WGS 84 (EPSG: 4326).

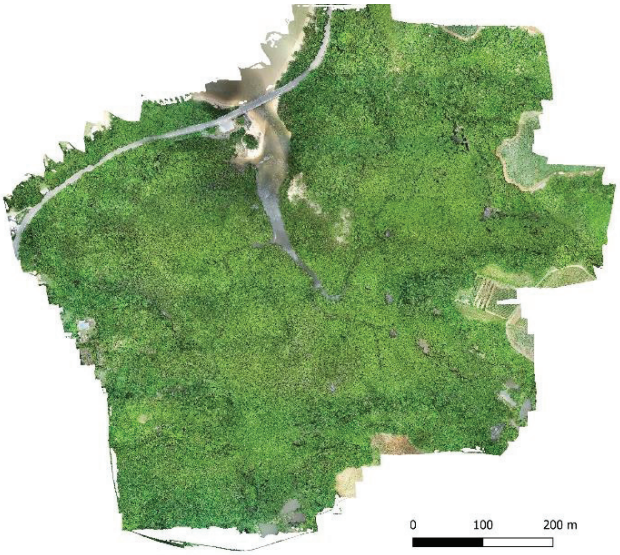

Figure 3.1 Orthomosaic photo from 80 m height

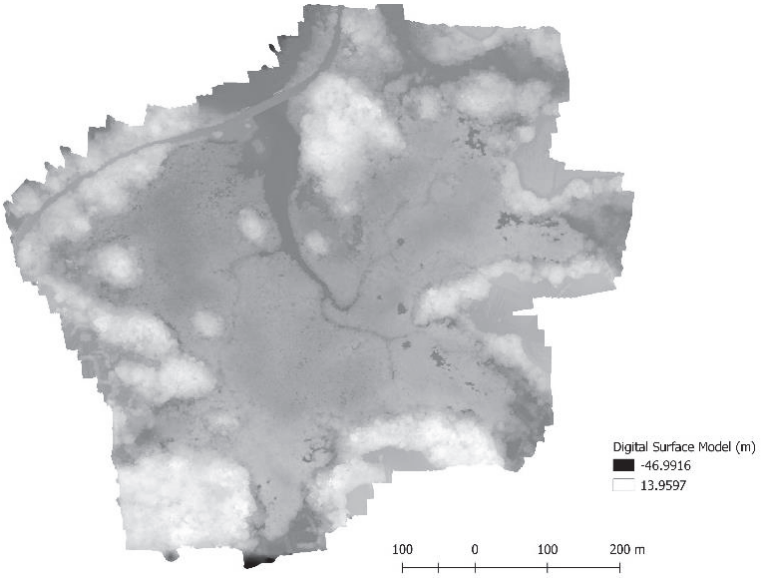

Figure 3.2 Digital Surface Model

3.2. Experiment results for mangrove mapping

3.2.1. The Results of Hyper-parameter tuning for Mangrove Distribution

This section describes the hyperparameter tuning for the input dataset to evaluate the performance of the model for the classification of mangrove distribution. The experiment of hyper-parameter tuning is described in Table 2.3. In the experiment, the batch size, the base number of kernels, and the learning rate were all differently setup to evaluate better performance and speed up the processing. According to the results of hyperparameter tuning, the T1 model was the best classification result for mangrove mapping. The detailed tuning results are as shown in Table 3.1.

Table 3.1 The results of Hyper-parameter tuning

Experiment	**Hyper-parameter tuning**	**Overll accuracy**
T1	Batch size = 32, base kernel = 24 Learning rate = 0.0002	0.957
T2	Batch size = 32, base kernel = 32 Learning rate = 0.0002	0.957
T3	Batch size = 24, base kernel = 32 Learning rate = 0.0001	0.956
T4	Batch size = 24, base kernel = 16 Learning rate = 0.0001	0.955
T5	Batch size = 24, base kernel = 64 Learning rate = 0.0001	Out of memory
T6	Batch size = 16, base kernel = 32 Learning rate = 0.0001	0.957
T7	Batch size = 32, base kernel = 16 Learning rate = 0.0001	0.956

As a hyper-parameter tuning result of the U-Net model, the best performance results for mangrove classification are batch size of 32, number of base kernels 24, and the learning rate of 0.0002 through this study.

3.2.2. Classification results for Mangrove Distribution from U-Net

After training the model, the testing part was applied to evaluate the classification result of the model. The results of the classification for the testing part are presented in Table 3.2. Figure 3.3 shows the classification result: Green = True Positive (TP), Blue = False Positive (FP), Red = False Negative (FN), White = True Negative (TN), respectively.

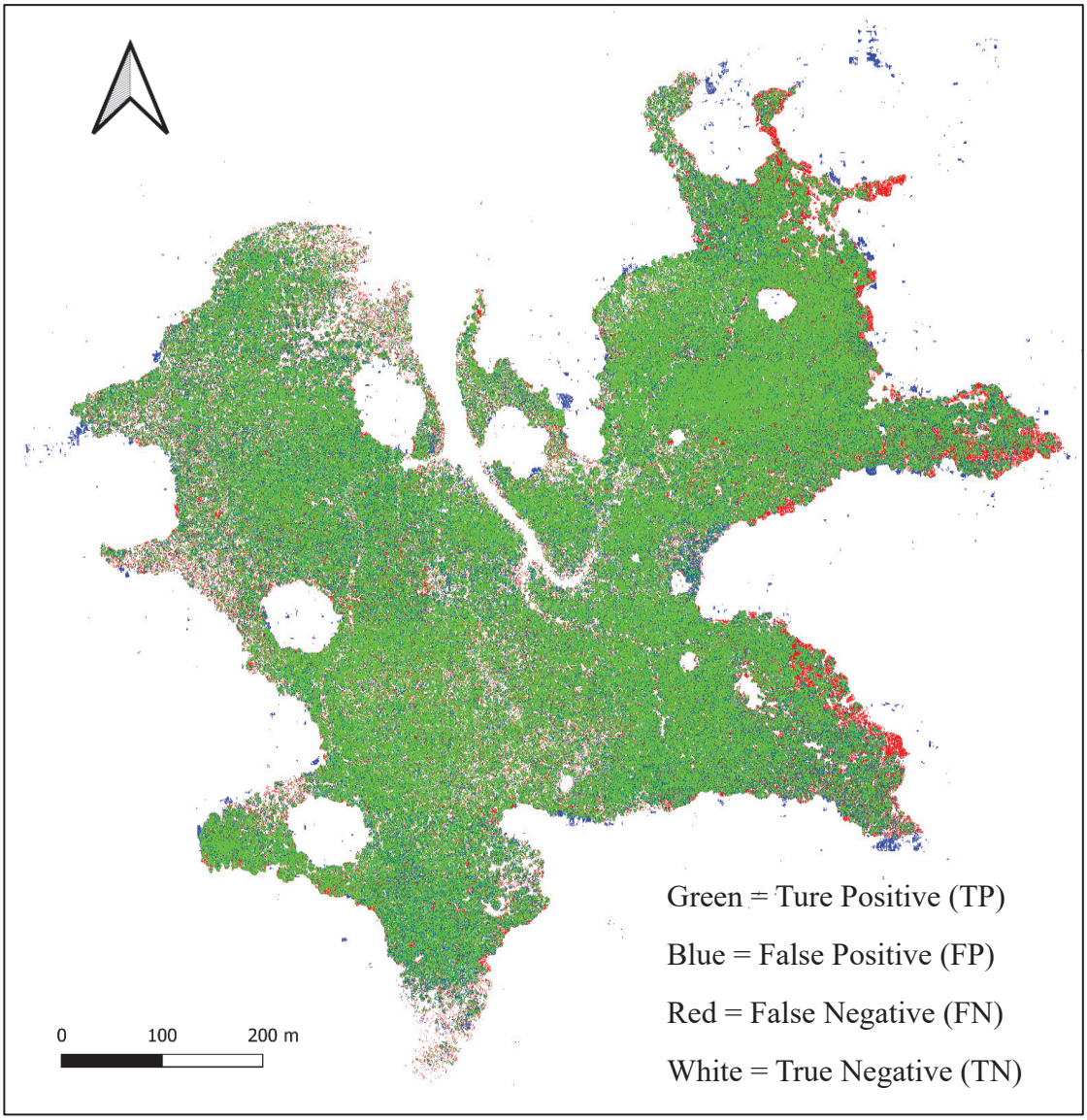

Figure 3.3 Classified Image: Green = TP, Blue = FP, Red = FN, White = TN

Table 3.2 The classification results from testing part

Experiment	Overll accuracy	Precision	Recall	F1 score	IoU	Kappa
T1	0.957	0.827	0.866	0.846	0.733	0.821
T2	0.957	0.834	0.849	0.841	0.726	0.816
T3	0.956	0.835	0.845	0.84	0.735	0.815
T4	0.955	0.817	0.858	0.837	0.720	0.811
T5	Out of memory	Out of memory	Out of memory	Out of memory	Out of memory	Out of memory
T6	0.957	0.841	0.846	0.843	0.729	0.819
T7	0.956	0.837	0.838	0.837	0.720	0.812

3.2.3. Mangrove distributed areas though this study

To assess the current mangrove-distributed areas of the Fukido river estuary, this study calculated the accrual mangrove areas that was derived from the classified image of the U-Net model classification. This study supports that the mangrove-distributed area of the Fukido river estuary is 15.05 hectares (ha). Before calculating the mangrove distributed area, the coordinate system of the classified image was changed into the UTM zone (WGS 84/UTM 51 N for Ishigaki Island areas) to calculate the cell count for mangrove pixels. For area calculation, the classified images of mangrove area and the resolution of the classified image were first calculated, and then the area value was divided by 10,000 to change ha for mangrove distribution. The procedures for the detailed area calculation in this study are provided in Table 3.3.

Table 3.3 shows the procedures of detail area calculation for mangrove classification

No.	Value (raster)	Count (classified pixel)	X resolution (m)	Y resolution (m)	Area (ha)
1	255	167,223,663	0.03	0.03	15.05

Note: X , Y resolution = the resolution of the classified image

3.3. Classification results for Species distribution from Random Forest

Based on the classification result of random forest, the overall accuracy of species distribution map was 82.7 % and the f1-score 0.82 with the number of trees 500 in random forest classification. According to species-level classification result, the *B.gymnorhiza* was dominantly distributed over the study area, in addition, the *R.stylosa* was dominant not only along the creek (river) but also in some high ground area (Figure 3.4).

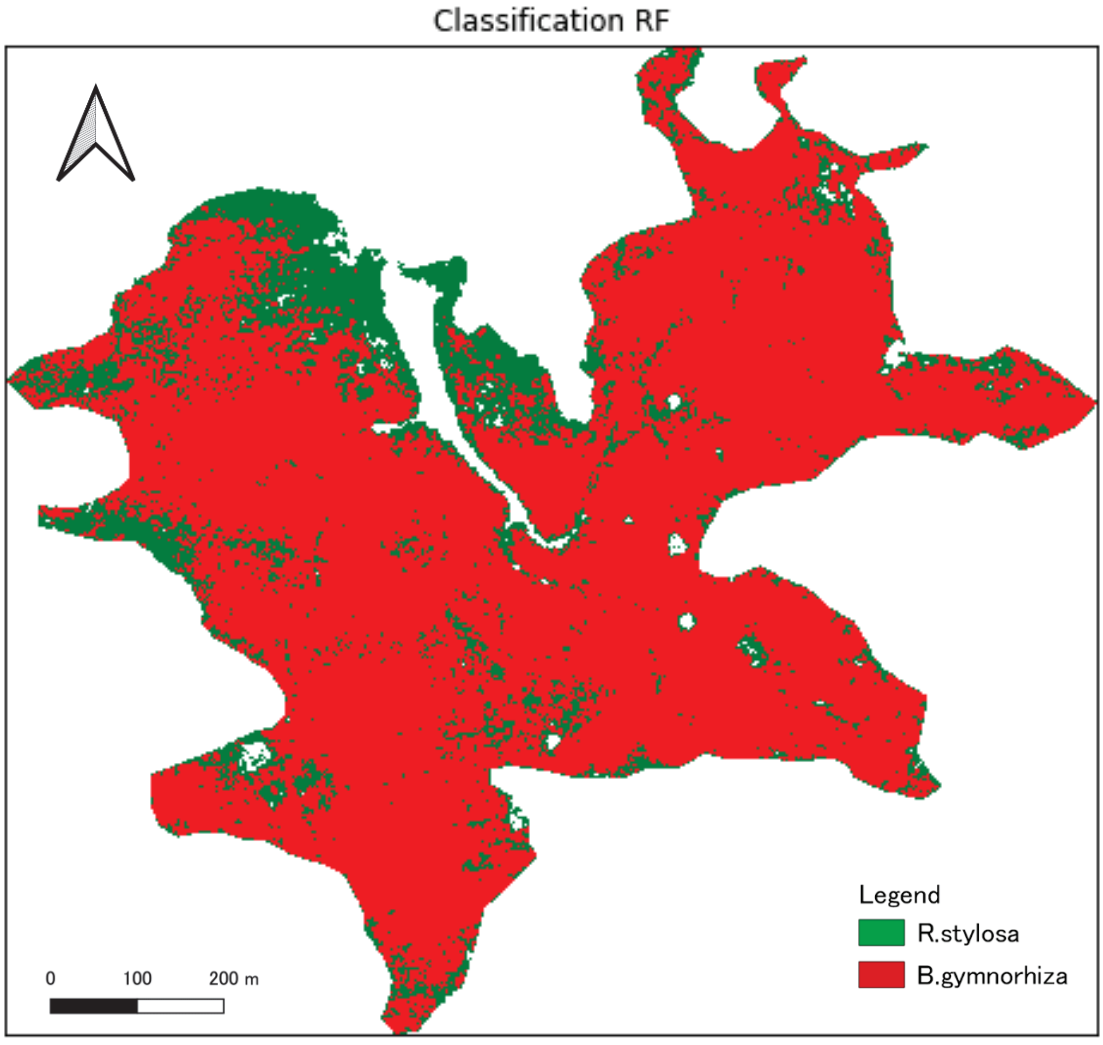

Figure 3.4 Classified image using Random Forest classifier

3.4. Results from Tree Survey

Of the total of 9 sample plots (the size of each plot is 10 m radius) for tree data collection, mixed two-species areas and mono-species areas were observed throughout the field survey. In total, 699 trees were sampled within 9 plots, as shown in Figure 3.5 and Table 3.4. Five plots (plot 1, plot 4, plot 6, plot 7, and plot 8) were located near the creek (river) within the study area, while four plots (plot 2, plot 3, plot 5, and plot 9) were at the landward site (Figure 3.5). The pie chart in the figure means the number of trees distributed within the plots; the colors green and red represent R. stylosa and B. gymnorrhiza, respectively. According to Table 3.4, plots 2 and 3 have the highest tree density (over 100 trees/plot) of the other plots, and plot 9 has the lowest tree density (only 39 trees/plot) in this study.

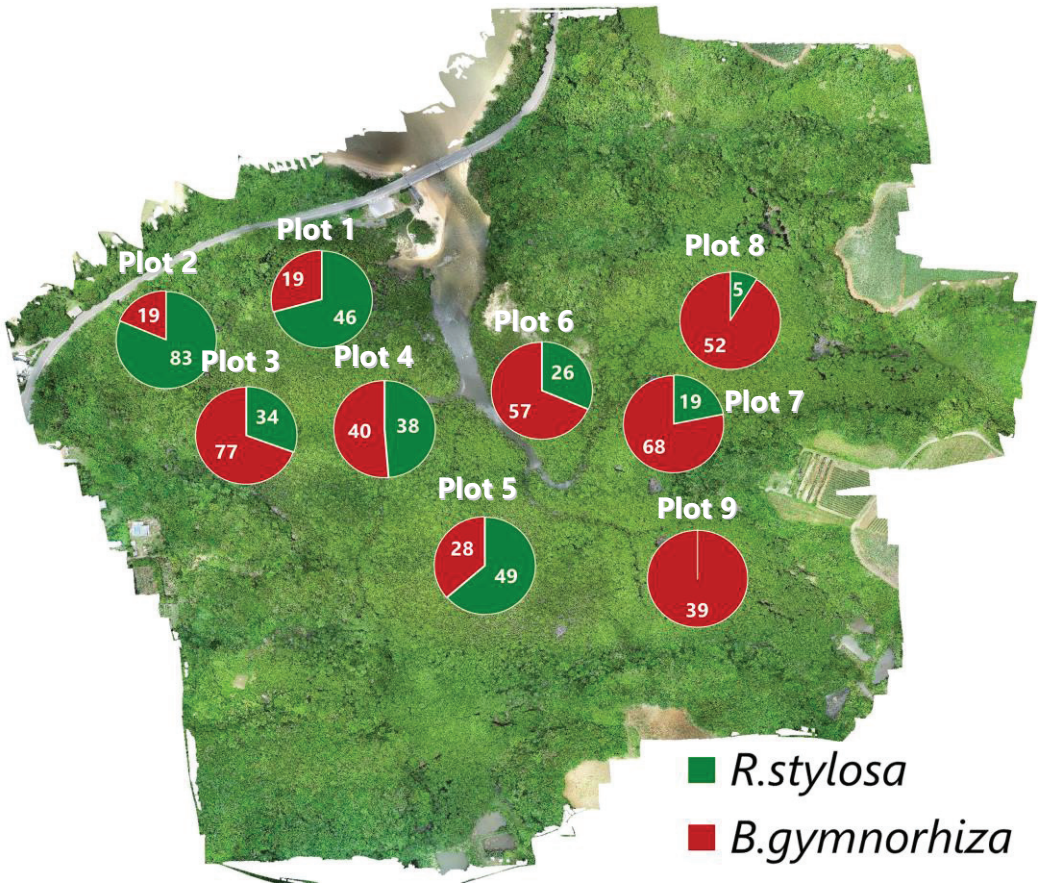

Figure 3.5 The location of the sample plots

Tabel 3.4 The number of trees recorded from field observation

Plots	R.stylosa	B.gymnorhiza	Total
Plot 1	46	19	65
Plot 2	83	19	102
Plot 3	34	77	111
Plot 4	38	40	78
Plot_5	49	28	77
Plot 6	26	57	83
Plot 7	19	68	87
Plot 8	5	52	57
Plot 9	0	39	39

The average and standard deviation of tree diameter and height were first calculated from the data of the tree survey to analyze the species distribution within the plots. The characteristics of *R. stylosa* and *B. gymnorrhiza* were shown in Table 3.2 and Table 3.3. From Table 3.2, the maximum and minimum tree diameters of the plots for *R.stylosa* are 14.2 cm and 5.4 cm, and the maximum and minimum tree heights are 881 cm and 331 cm, respectively. From Table 3.3, the maximum and minimum tree diameters for *B.gymnorhiza* were 17.9 cm and 1.5 cm in plot 1. The maximum and minimum tree heights are 1011 cm in plot 6, and 282 cm in plot 5, respectively.

Table 3.5 Statistics for *Rhizophora stylosa* trees within the plots (the unit of diameter and height are cm; STD means standard deviation)

Plots	Mean diameter	STD	Max diameter	Min diameter	Mean height	STD	Max height	Min height	rate (%)
Plot 1	10.1	1.8	14.2	5.8	617.4	83.4	757.0	388.0	70.8
Plot 2	7.2	1.5	8.8	5.4	452.4	45.6	504.0	374.0	81.4
Plot 3	9.1	1.4	11.8	7.7	688.4	71.1	810.0	608.0	30.6
Plot 4	10.3	0.6	10.9	9.5	691.6	26.6	741.0	671.0	48.7
Plot 5	9.1	1.4	10.9	7.4	582.2	159.2	735.0	331.0	63.6
Plot 6	10.3	1.4	12.7	6.6	753.8	72.2	881.0	603.0	31.3
Plot 7	10.9	1.6	12.7	8.0	784.4	44.5	834.0	720.0	21.8
Plot 8	11.1	1.5	13.0	9.2	799.0	41.7	847.0	744.0	8.8
Plot 9	-	-	-	-	-	-	-	-	0.0

Table 3.6 Statistics for *Bruguiera gymnorrhiza* trees within the plots (the unit of diameter and height are cm; STD means standard deviation)

Plots	Mean diameter	STD	Max diameter	Min diameter	Mean height	STD	Max height	Min height	rate (%)
Plot 1	10.5	3.4	14.0	4.4	620.0	82.0	698	468	29.2
Plot 2	6.0	1.6	7.9	3.9	377.2	68.1	488	282	18.6
Plot 3	6.9	1.5	9.6	5.1	553.4	80.6	654	476	69.4
Plot 4	8.5	1.5	10.2	6.3	601.8	43.3	635	516	51.3
Plot 5	10.4	5.1	17.9	4.5	681.6	205.6	905	433	36.4
Plot 6	10.7	10.4	13.1	8.2	769.4	17.9	789	743	68.7
Plot 7	8.5	2.8	13.0	4.9	602.2	142.1	797	395	78.2
Plot 8	6.9	4.8	15.8	1.5	672.6	134.3	840	530	91.2
Plot 9	13.8	3.1	17.8	9.9	992.6	16.6	1011	968	100.0

Figure 3.6 shows the histogram of the tree height and diameter for each species. According to graphs on tree height, B.gymnorrhiza species have a linear distribution through the study area, but two peak distributions were found for R.stylosa species. The average height and diameter of B. gymonorhiza were 992.6 cm and 13.8 cm, while the average height and diameter of R. stylosa were 799.0 cm and 11.1 cm, respectively, in this study.

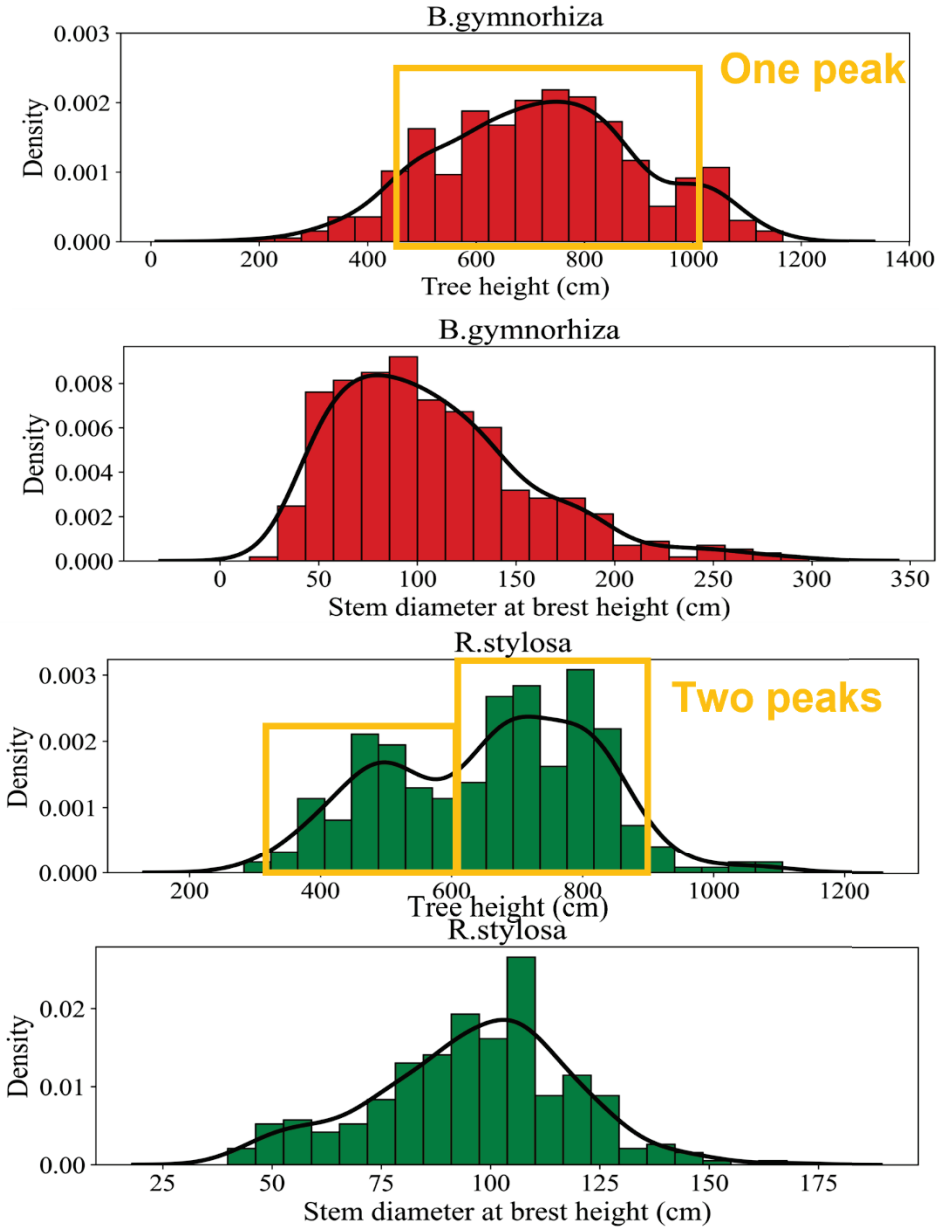

Figure 3.6. The distribution of R.stylosa and B.gymnorrhiza from field survey

3.5. Results of Water Level Data

As an environmental factor for mangrove species distribution, the relative inundation duration (RID) of each plot was calculated to analyze the inundation period (Table 3.7 and Figure 3.7). The results from the RID calculation show that the average percentage of RID in plot number 8 (73.3%) is higher than in the other plots. Suppose that the ground height of plot number 8 is nearly the same as that of the base station. In similarity, the average percentage of RID in plot 1 (67.5%), plot 4 (57.8%), plot 6 (61.2%), and plot 7 (67.1%) were recorded as high values. Plot numbers 1, 2, and 5 are the R. stylosa dominant areas, while the other plots are dominated by B. gymnorhiza (Figure 3.7).

Table 3.7. shows the average, standard deviation, maximum and minimum data of the water level data

Plots	Mean (%)	Standard Deviation (%)	Maximum (%)	Minimum (%)
Plot 1	67.5	2.2	71.4	66.1
Plot 2	44.0	5.2	49.2	38.8
Plot 3	36.2	0.0	36.2	36.2
Plot 4	57.8	0.0	57.8	57.8
Plot 5	40.9	5.2	47.5	34.9
Plot 6	61.2	2.8	64.8	57.0
Plot 7	67.1	3.3	71.3	63.0
Plot 8	73.3	3.6	78.7	70.0
Plot 9	42.2	6.5	50.0	34.1

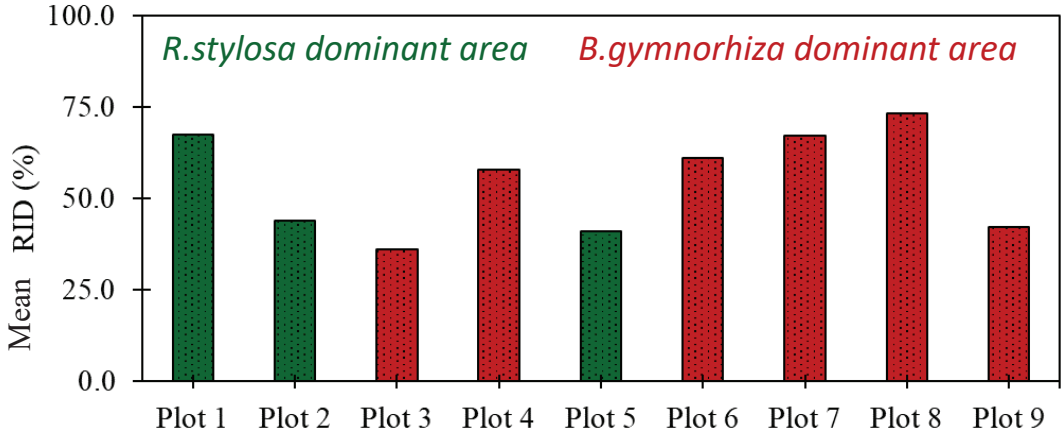

Figure 3.7 The mean relative inundation duration (RID) of the plots

Chapter 4 DISCUSSION

4.1. Convolutional Neural Network based classification for mangrove distribution

The two major challenges that could be faced when mangrove mapping with remote sensing techniques are: the first is related to accurate boundary demarcation of the mangrove area, and the second one is mixing with the other land trees, wet soil, and water. These factors would affect the accuracy of map classification [55]. To overcome such kinds of challenges, the extraction of mangrove extent was conducted by extracting texture information from drone imagery using the U-Net model under a CNN-based deep learning approach in this study.

4.1.1. Model performance through hyper-parameter tuning

For hyperparameter tuning, batch size, the number of base kernels, and the learning rate were decided after conducting several experiments for mangrove mapping with drone imagery because there is no exact information about the hyperparameters for mangrove distribution. Therefore, different hyper-parameters were set up to conduct different experiments for mangrove classification to evaluate the model performance of U-Net. As a hyperparameter tuning result of the U-Net model, the best performance parameters for mangrove classification are the batch size of 32, the number of base kernels 24, and the learning rate of 0.0002 throughout this study. The highest overall accuracy of these results was 95.7%, while the minimum overall accuracy of the other experiments was 95.5% with the same dataset (Table 3.1). Therefore, this study proposed drone imagery classification with the U-Net model for mangrove distribution under the complex land cover, and the trained model could also be applied to the other mangrove distributed areas of any region using drone imagery for intensive mangrove conservation and management.

4.1.2 Mangrove distributed area in the Fukido river estuary

According to Baloloy et al. (2021), the area of mangrove extent in the Fukido river was assessed based on automatic extraction from the mangrove vegetation index using sentinel imagery (10 m resolution). As a result, the mangrove extent area was about 20.04 ha. From this study, the current situation of the mangrove distributed area was successfully calculated based on the classified image. In addition, the

method of ground truth data creation used by this study could apply to the other mangrove distributed areas for sustainable mangrove monitoring and management because it could provide accurate ground truth information, for example, even in the gap between two trees in the mangrove distributed area. Although the mangrove area exists for about 20.04 ha in the Fukido river estuary according to a previous study with satellite imagery, this study supports that the current mangrove tree-distributed area is 15.05 ha (as shown in Table 3.3). On the other hand, the other remaining areas excluding the mangrove areas was the mangrove degraded areas, and some mountainous areas within the Fukido river mangrove.

4.2. Mangrove species Distribution using Random Forest

In general, *R.stylosa* is dominant along the creek (river, low ground area), and distribution pattern of *B.gymnorhiza* is in medium ground and high ground area (Figure 3.8) [56]. According to results of species classification, the *B.gymnorhiza* was dominantly distributed over the study area, in addition, the *R.stylosa* was dominant not only along the creek (river) but also in some high ground area. From these results, the overall accuracy of the species classification was 82.7 % with the number of trees 500 in random forest classification.

樹種 Species	根の形状 Root Shape	抵抗力 Drag Force	樹高 Tree Height	生育場所 Breeding Place	耐塩性 Salt Tolerance
 B.gymnorhiza (オヒルギ)	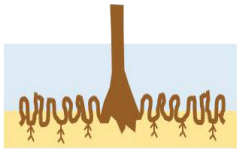 膝根 Knee roots	中 moderate	10m	中心群落 middle	中 moderate
 R.stylosa (ヤエヤマヒルギ)	 支柱根 Prop roots	高 high	6m	中心前面群落 middle, seaward	高 high

Figure 3.8 The growing places for *B.gynorhiza* and *R.stylosa*

4.3. Species Distribution from field observation data

4.3.1. Competition between R.stylosa and B.gymnorhiza

According to the results of tree height analysis, the height distribution of R. stylosa has a non-linear distribution, while B. gymnorhiza has a linear distribution (Figure 3.6). Among the plots, plot 1, plot 2, and plot 5 were R. stylosa-dominated areas, while plot 3, plot 4, plot 6, plot 7, plot 8, and plot 9 were B. gymnorhiza-dominated areas (Figure 4.1). The pie chart on the figure means the species-dominated areas for each plot: the colors yellow and white from the plot name are R. stylosa dominated areas and B. gymnorhiza dominated areas, respectively. Figure 4.2 shows the relationship between the minimum height of R. stylosa and the percentage of R. stylosa at each plot. The minimum height of the R.stylosa in plot 3, plot 4 and plot 6, plot 7, and plot 8 (over 600 cm) was taller than in plot 1, plot 2, and plot 5 (under 400 cm) (Figure 4.2). The areas where the minimum tree height of R. stylosa was over 600 cm were located in the B. gymnorhiza-dominated area. It indicates that part of the R.stylosa in the B.gymnorhiza-dominated areas would survive under the competition with B.gymnorhiza by increasing the tree height.

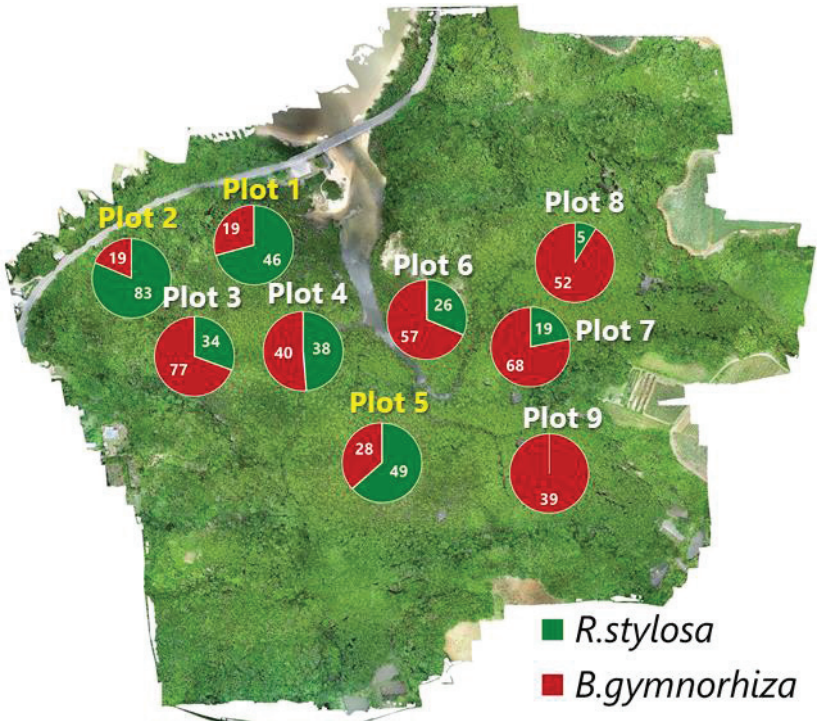

Figure 4.1 Two species distributed area in each plot

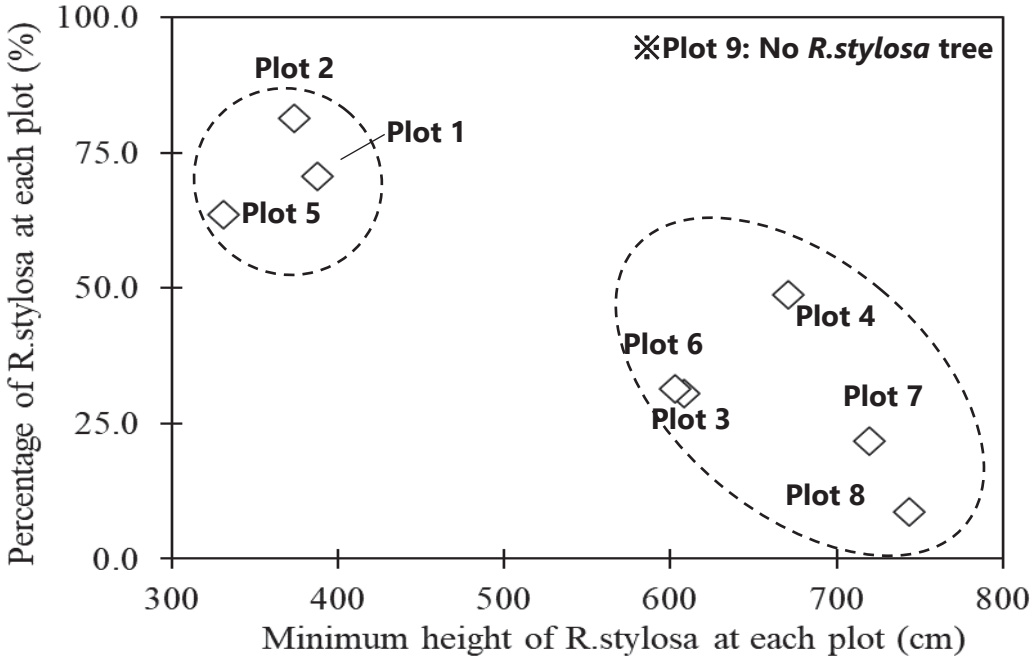

Figure 4.2 the relationship between the minimum height of R.stylosa and the percentage of R.stylosa at each plot (no R.stylosa species exist in plot 9)

Based on the results from the relative inundation duration (RID) of each plot, plot 8 (73.3%), which is located in the B. gymnorhiza-dominated areas, has the highest RID values of the other plots (Figure 3.3). In addition, the R. stylosa-dominated areas of plot 1, plot 4, and plot 7 were also observed as high RID values. From these results, there was no significant relationship between the distribution of species and the relative inundation period (RID) in this study because of some parts of R. stylosa species could survive even at high ground level.

4.3.2. Species distribution with tree density

According to Herman H. Shugart (1984) [57], the distribution of species in land forests could change based on their successional status regarding the growth rate changes due to the effect of environmental gradients. Figure 4.3 shows the tree density distributed area in each plot: the green and red from the bar chat are *R.stylosa* and *B.gymnorhiza,* respectively. According to the analysis of tree density for all plots, plot 1 and plot2 was the highest tree density, while plot 1, plot 8 and plot 9 were the lowest tree density though this study. The location of plot 2 was in

R.stylosa dominated area, while the plot 3 was in *B.gymnorhiza* dominated area (Figure 4.3). According to these results, the percentage of *R.stylosa* decreases from plot 2 to plot 3 (Figure 4.4). In addition, species transition occurred from plot 2 to plot 3 when analyzing the minimum height of *B.gymnorhiza* and the minimum height of *R.stylosa* at each plot (Figure 4.5). In conclusion, from these results, indicate that some parts of the R.stylosa could survive under the competition with B.gymnorhiza.

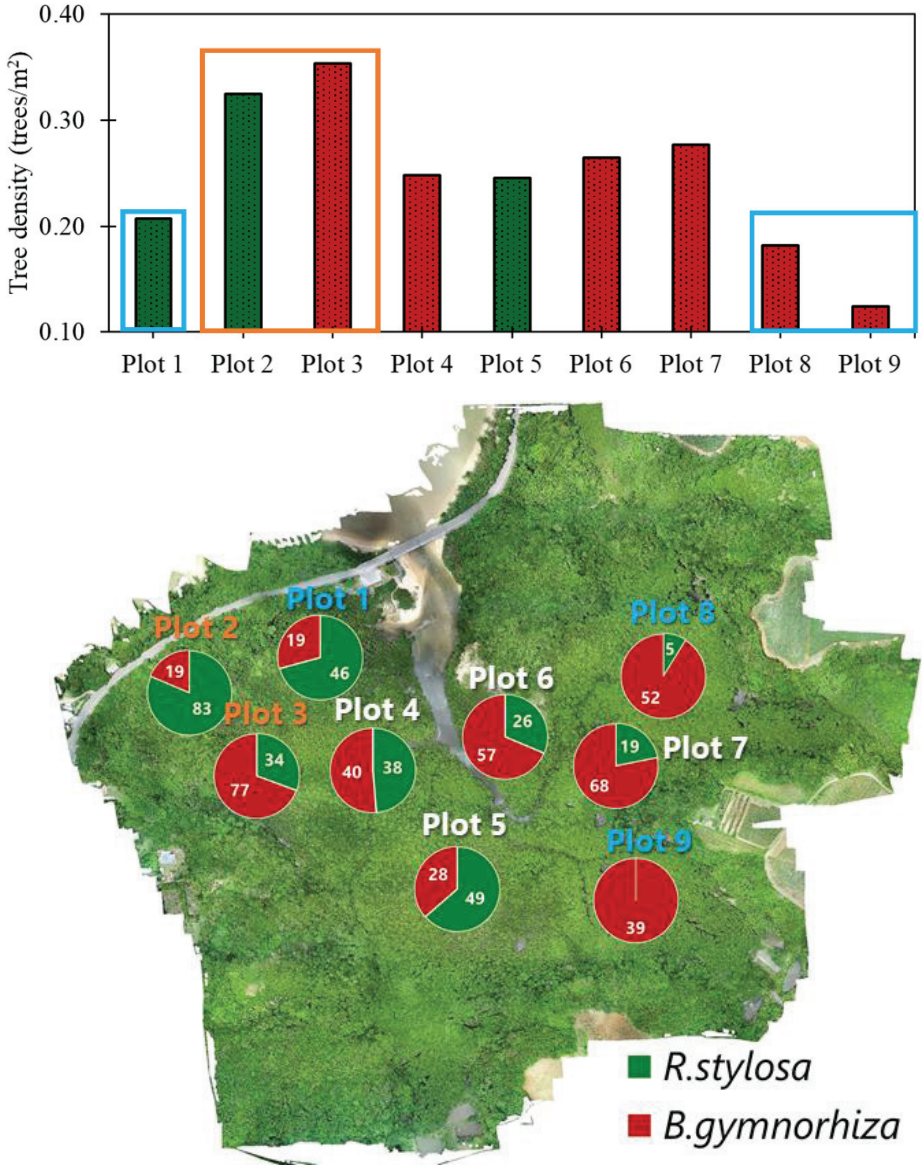

Figure 4.3 (a) Tree density (trees/m^2) of all plots, (b) the characteristics of *R.stylosa* distribution in each plot by tree density

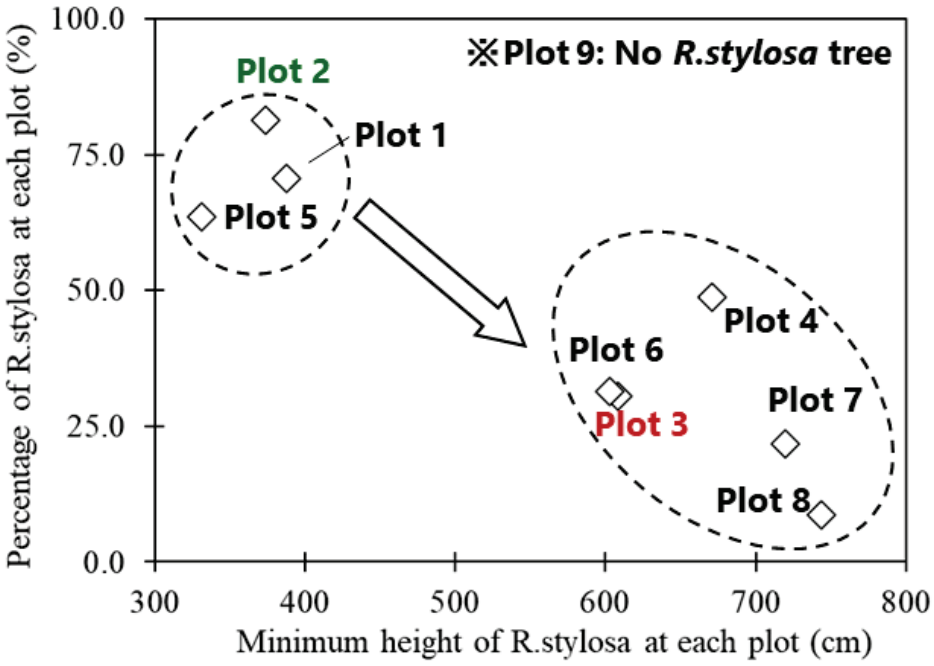

Figure 4.4 the relationship between the minimum height of R.stylosa and the percentage of R.stylosa at each plot

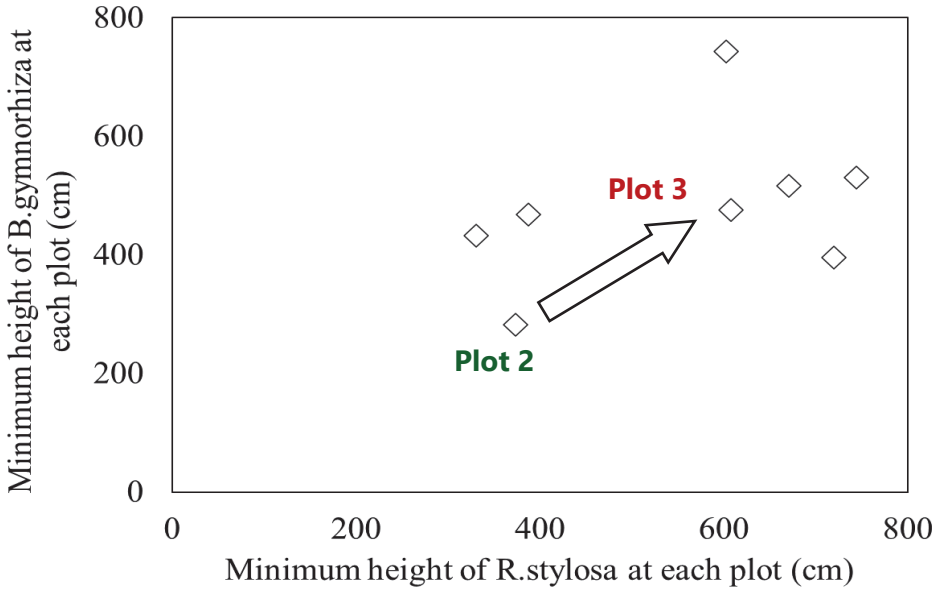

Figure 4.5 species transition occurred between plot 2 and plot

CHAPTER 5 CONCLUSIONS AND LIMITATION

5.1. Conclusions

From this study, the mangrove distribution was extracted using drone imagery (rgb images) with U-Net based classification in the Fukido river estuary, which was the first application of U-Net for the classification of the mangrove distribution. Based on the hyper-parameter tuning results, the best performance for the classification of mangrove distribution using the U-Net model achieved an overall accuracy of 95.7 %. In addition, this study showed that the current mangrove tree-distributed area in the Fukido river estuary was 15.05 ha. Moreover, the creation of ground truth data based on ISO Unsupervised Classification could be helpful information to assist in creating the ground truth (label) data for the other mangrove scattered regions. Therefore, this study proposed drone imagery classification with the U-Net model for mangrove distribution under the complex land cover, and the trained model could also be applied to the other mangrove distributed areas of any region using drone imagery for intensive mangrove conservation and management.

On the other hand, according to the result of species level classification, the *B.gymnorhiza* was dominantly distributed over the study area. In addition, the *R.stylosa* was dominant not only along the creek (river) but also in some high ground areas. By integrating with field observation, the study observed some parts of R.styosa could survive under the competition with *B.gymnorhiza* in the *B.gymnorhiza* area by increasing the tree height. Moreover, according to the results of relative tide inundation duration (RID), there was no significant relationship between the distribution of species and the relative inundation period (RID) in this study because of the ability of *R. stylosa* species to survive even at high ground level.

The findings of this study provide the current information for mangrove extent and species-level mapping with high-resolution drone imagery including species distribution changes by integrating with field observation data for future mangrove management and conservation in the Fukido river mangrove.

5.2. Limitation

The application of the U-Net model using drone imagery and ground truth data used in this study to the other mangrove environments is necessary to assess the consistency of the method.

REFERENCES

1. C.Giri, E.Ochieng, L.L. Tiezen, Z. Zhu, A. Singh, T.Loveland, Masek and N. Duke, Status and distribution of mangrove forests of the world using earth observation satellite data, Global Ecology and Biogeography, (Global Ecol. Biogeogr.)(2011) 20, 154-159
2. Alongi, D.M. (2009) Introduction in the energetics of mangrove forests. Springer Science and Business Media BV, New York.
3. Donato DC, Kauffman JB, Murdiyarso D et al. Mangroves among the most carbon rich forests in the topics. Nat. Geosci. 4, 293-297 (2011).
4. Matsui, M. Suekuni, J., Nogami, M., Havanond, S. Salikul, P., (2010). Mangrove rehabilitation dynamics and soil organic carbon change as a result of full hydraulic restoration and regarding of a previously intensively managed shrimp pond. Wetland Ecol. Manag., Vol. 18: 233-242
5. Edward Zimudzi, Ian Sanders, Nicholas Rollings & Christian Omlin (2019) Segmenting mangrove ecosystems drone images using SLIC superpixels, Geocarto International, 34:14, 1648-1662, DOI: 10.1080/10106049.2018.1497093
6. Komiyama, A.; Ong, J.E.; Poungparn, S. Allometry, biomass, and productivity of mangrove forests: A review. Aquatic Bot. 2008, 89, 128–137.
7. Duke, N.C., Meynecke, J.-O., Dittmann, S., Ellison, A.M., Anger, K., Berger, U., Cannicci, S., Diele, K., Ewel, K.C., Field, C.D., Koedam, N., Lee, S.Y., Marchand, C., Nordhaus, I. & Dahdouh-Guebas, F. (2007) A world without mangroves? Science, 317, 5834, 41–42.
8. Spalding, M.D., Mami Kainumaand Lorna Collins. (Eds); World Atlas of Mangroves. 2010.
9. RICHARD M. LUCASa, ANTHEA L. MITCHELL , AKE ROSENQVIST, CHRISTOPHE PROISY, ALEX MELIUS, and CATHERINE TICEHURST, The potential of L-band SAR for quantifying mangrove characteristics and change: case studies from the tropics, Aquatic Conserv: Mar. Freshw. Ecosyst. 17: 245–264 (2007)

10. Gilman, E., Ellison, J., Duke, N.C. & Field, C. (2008) Threats to mangroves from climate change and adaptation options: a review. Aquatic Botany, 89, 2, 237–250.
11. Giri C, Ochieng E, Tieszen LL, Zhu Z, Singh A, Loveland T, et al. Status and distribution of mangrove forests of the world using earth observation satellite data. Global Ecology and Biogeography. 2011; 20 (1):154–159.
12. Spalding, M.D., Mami Kainumaand Lorna Collins. (Eds); World Atlas of Mangroves. 2010.
13. Miyawaki, A. "Socio-economic aspects of mangrove vegetation in Japan." In Man in the mangroves: the socio-economic situation of human settlements in mangrove forests: proceedings of a workshop held in Nong Nuch Village, Pattaya, Thailand, 27-31 May 1985/edited by P. Kunstadter...[et al.]. Tokyo, Japan: The United Nations University, c1986., 1986.
14. Vannucci, M. (2002). Indo-west Pacific mangroves. In Mangrove ecosystems (pp. 123-215). Springer, Berlin, Heidelberg.
15. Furakawa, K. and Baba, S. (2000) "Effects of sea level rise on Asian Mangroves Forest", in Minura, N. and Yokoki, H.(eds) Proceedings of the APN/SURVAS/LOICZ Joint Conference on Coastal Impacts of Climate Change and Adaptation in the Asia-Pacific Region, 14-16 November 2000, Kobe, Japan
16. Maxwell, G.(2009) "Review comments on draft text for "World Altas of Mangrove"
17. Bayan Alsaaideh, Ahmad Al-Hanbali, Ryutaro Tateishi, Toshiyuki Kobayashi, Nguyen Thanh Hoan, Mangrove Forests Mapping in the Southern Part of Japan Using Landsat ETM+ with DEM, Journal of Geographic Information System, 2013, 5, 369-377, http://dx.doi.org/10.4236/jgis.2013.54035.
18. Sharma, S., Yasuoka, J., Nakamura, T., Watanabe, A., Nadaoka, K. 2014. The Role of A.B. Baloloy, et al. ISPRS Journal of Photogrammetry and Remote Sensing 166 (2020) 95–117 116 hydroperiod, soil moisture and distance from the river mouth on soil organic matter in Fukido

19. B.Baloloy, Ariel C. Blanco, Raymund Rhommel C. Sta.Ana, Kazuo Nadaoka, Development and application of a new mangrove vegetation index (MVI) for rapid and accurate mangrove mapping, Volume 166, August 2020, Pages 95-117, https://doi.org/10.1016/j.isprsjprs.2020.06.001
20. Astrid J. Hsu, Joy Kumagai, Fabio Favoretto, John Dorian , Benigno Guerrero Martinez and Octavio Aburto-Oropeza, Driven by Drones: Improving Mangrove Extent Maps Using High-Resolution Remote Sensing, Remote Sens. 2020, 12, 3986; doi:10.3390/rs12233986
21. Juan Carlos Rocha, Reinette (Oonsie) Biggs. Mangrove transitions. In: Regime Shifts Database, www.regimeshifts.org. Last revised 2017-08-21 12:35:18 GMT.
22. Wang, L.; Jia, M.; Yin, D.; Tian, J. A review of remote sensing for mangrove forests: 1956–2018. Remote Sens. Environ. 231, 2019. 24.
23. Yoshino, K.; Pham, T.D.; Bui, D.T.; Friess, D.A.; Yokoya, N.; Bui, D.T.; Yoshino, K.; Friess, D.A. Remote sensing approaches for monitoring mangrove species, structure, and biomass: Opportunities and challenges. Remote Sens. 11, 1–24, 2019
24. Guo, M.; Yu, Z.; Xu, Y.; Huang, Y.; Li, C. ME-Net: A Deep Convolutional Neural Network for Extracting Mangrove Using Sentinel-2A Data. Remote Sens. 2021, 13, 1292. https://doi.org/10.3390/ rs13071292
25. Maggiori, E.; Tarabalka, Y.; Charpiat, G.; Alliez, P. Convolutional neural networks for large-scale remote-sensing image classification. IEEE Trans. Geosci. Remote Sens. 2016, 55, 645–657. [CrossRef]
26. Bei, W.; Guo, M.; Huang, Y. A Spatial Adaptive Algorithm Framework for Building Pattern Recognition Using Graph Convolutional Networks. Sensors 2019, 19, 5518. [CrossRef]
27. Liu, Z.; Li, X.; Luo, P.; Loy, C.-C.; Tang, X. Semantic image segmentation via deep parsing network. In Proceedings of the IEEE International Conference on Computer Vision, Santiago, Chile, 5–7 December 2015.
28. Xu, Y.; Xie, Z.; Feng, Y.; Chen, Z. Road extraction from high-resolution remote sensing imagery using deep learning. Remote Sens. 2018, 10, 1461. [CrossRef]

29. Chen, S.; Wang, H.; Xu, F.; Jin, Y.Q. Target Classification Using the Deep Convolutional Networks for SAR Images. IEEE Trans. Geosci. Remote Sens. 2016, 54, 4806–4817. [CrossRef]
30. Zhao, W.; Du, S. Spectral-spatial feature extraction for hyperspectral image classification: A dimension reduction and deep learning approach. IEEE Trans. Geosci. Remote Sens. 2016, 54, 4544–4554. [CrossRef]
31. Xu, Z.; Xu, X.; Wang, L.; Yang, R.; Pu, F. Deformable ConvNet with Aspect Ratio Constrained NMS for Object Detection in Remote Sensing Imagery. Remote Sens. 2017, 9, 1312. [CrossRef]
32. Krizhevsky, A.; Sutskever, I.; Hinton, G. ImageNet Classification with Deep Convolutional Neural Networks; NIPS. Curran Associates Inc.: Lake Tahoe, NV, USA, 2012.
33. Yichao Dong, Kun Yu, and Wenxin Hu. 2021. GC-UNet: An Improved UNet Model for Mangrove Segmentation Using Landsat8. In The 2021 3rd International Conference on Big Data Engineering (BDE 2021), May 29–31, 2021, Shanghai, China. ACM, New York, NY, USA, 6 pages. https: //doi.org/10.1145/3468920.3468928
34. Corina Iovan, Michel Kulbicki, Eric Mermet, DEEP CONVOLUTIONAL NEURAL NETWORK FOR MANGROVE MAPPING, DOI: 10.1109/IGARSS39084.2020.9323802
35. Guo, Y.; Liao, J.; Shen, G. Mapping Large-Scale Mangroves along the Maritime Silk Road from 1990 to 2015 Using a Novel Deep Learning Model and Landsat Data. Remote Sens. 2021, 13, 245. https:// doi.org/10.3390/rs1302024
36. Xu, Y.; Xie, Z.; Feng, Y.; Chen, Z. Road extraction from high-resolution remote sensing imagery using deep learning. Remote Sens. 2018, 10, 1461. [CrossRef]
37. Chen, L.-C.; Papandreou, G.; Kokkinos, I.; Murphy, K.; Yuille, A.L. Deeplab: Semantic image segmentation with deep convolutional nets, atrous convolution, and fully connected crfs. IEEE Trans. Pattern Anal. Mach. Intell. 2017, 40, 834–848.

38. Badrinarayanan, V.; Kendall, A.; Cipolla, R. Segnet: A deep convolutional encoder-decoder architecture for image segmentation. IEEE Trans. Pattern Anal. Mach. Intell. 2017, 39, 2481–2495. [CrossRef]
39. Long, J.; Shelhamer, E.; Darrell, T. Fully Convolutional Networks for Semantic Segmentation. In Proceedings of the IEEE Conference on Computer Vision and Pattern Recognition, Boston, MA,
40. Zheng, S.; Jayasumana, S.; Romera-Paredes, B.; Vineet, V.; Su, Z.; Du, D.; Huang, C.; Torr, P.H. Conditional Random Fields as Recurrent Neural Networks. In Proceedings of the IEEE International Conference on Computer Vision, Santiago, Chile, 7–13 December 2015
41. Muditha K. Heenkenda, Karen E. Joyce, Stefan W. Maier and Renee Bartolo, Mangrove Species Identification: Comparing WorldView-2 with Aerial Photographs, Remote Sens. 2014, 6, 6064-6088; doi:10.3390/rs6076064
42. Kuenzer, C.; Bluemel, A.; Gebhardt, S.; Quoc, T.V.; Dech, S. Remote Sensing of Mangrove Ecosystems; A Review. Remote Sens. 2011, 3, 878-928
43. Pham, T.D.; Bui, D.T.; Yoshino, K., Le, N.N. Optimized Rule-Based Logistic Model Tree Algorithm for Mapping Mangrove Species Using ALOS PALSAR Imagery and GIS in the Tropical Region. Environ. Earth Sci. 2018, 77, 1-13.
44. Coa, J.; Leng, W.; Liu, K.; Liu, L.; He, Z.; Y. Object-Based Mangrove Species Classification Using Unmanned Aerial Vehicle Hyperspectral Images and Digital Surface Models. Remote Sens. 2018, 10, 89.\
45. Arasumani, M.; Singh, A.; Bunyan, M.; Robin, V. Testing the Efficacy of Hyperspectral (AVIRIS-NG), Multispectral (Sentinel 2) and Radar (Sentinel 1) Remote Sensing Images to Detect Native and Invasive Non-Native Trees. Biol. Invasions 2021, 1-17.
46. Naidoo, L.; Cho, M.A.; Mathieu, R.; Asner, G. Classification of Savanna Tree Species, in the Greater Kruger National Park Region, by integrating Hyperspectral and LiDAR Data in a Random Forest Mining Environment. ISPRS J. Photogramm.Remote Sens. 2012, 69 167-179

47. Behera, M.D.; Barnwal, S.; Paramanik, S.; Das, P.; Bhattyacharya, B.K.; Jagadish, B.; Roy, P.S.; Ghosh, S.M.; Behera, S.K. Species Level Classification and Mapping of a Mangrove Forest Using Random Forest – Utilisation of AVIRIS-NG and Sentinel Data. Remote Sens. 2021, 13, 2027. https://doi-org/10.3390/rs13112027
48. Kauffman, J.B. and Donato, D.C. 2012 Protocols for the measurement, monitoring and reporting of structure, biomass and carbon stocks in mangrove forests. Working Paper 86. CIFOR, Bogor, Indonesia
49. Ronneberger et al., Clinically Applicable Segmentation of Head and Neck Anatomy for Radiotherapy: Deep Leaning Algorithm Development and Validation Study, 2021,https://preprints.jmir.org/preprint/26151
50. Breiman, L. (2001). Random forests. Machine Learning, 45, 5-32
51. Guo, L., Ghehata, N., Mallet, C., & Boukir, S. (2011). Relevance of airborne lidar and multispectral image data for urban scene classification using random forest. ISPRS Journal of Photogrammetry and Remote Sensing, 66, 56-66
52. Elhadi, A., Onisimo, M., John, O., & Elfatih, M. A. R. (2014). Land-use/ cover classification in a heterogeneous coastal landscape using RapidEye imagery: evaluating the performance of random forest and support vector machines classifier. International Journal of Remote Sensing, 35, 3440-3458
53. Eisavi, V., Homayouni, S., Yazdi, A.M. et al. Land cover mapping based on random forest classification of multitemporal spectral and thermal images. Environ Monit Assess 187, 291 (2015). http:s//doi.org/10.1007/s10661-015-4489-3
54. Ghosh, S.M.; Behera, M.D.; Paramanik, S. Canopy Height Estimation Using Sentinel Images thought Machine Learning Models in a Mangrove Forest. Remote Sens. 2020, 12, 1519.
55. Adam, E.; Mutanga, O.; Rugege, D. Multispectral and hyperspectral remote sensing for identification and mapping of wetland vegetation: A review. Wetl. Ecol. Manag. 2010, 18, 281–296
56. Yukira MOCHIDA, Kiyoshi FUJIMOTO, Toyohiko MIYAGI, Shuichi ISHIHARA, Tamon MUROFUSHI, Takao KIKUCHI, Paiboon

PRAMOJANEE, A Phytosociological Study of the Mangrove Vegetation in the Malay Peninsula, TROPICS Vol.8(3): 207-220, Issued May, 1999

57. Herman H. Shugart (1984), A Theory of Forest Dynamics, The Ecological Implication of Forest Succession

APPENDICES

Appendix 1 The number of trees that collected from field survey (for example, total number of trees are 699) (R.s = *R.stylosa*, B.g = *B.gymnorhiza*)

No.	Species Name	DBH(cm)	Height(cm)
1	R.s	10.929	660
2	B.g	9.262	565
3	R.s	12.53	705
4	B.g	7.128	545
5	R.s	10.845	665
6	R.s	9.059	655
7	B.g	19.965	630
8	B.g	12.078	592
9	R.s	10.817	683
10	R.s	10.577	689
11	R.s	7.673	566
12	R.s	12.265	646
13	R.s	10.477	637
14	R.s	9.554	628
15	R.s	9.14	624
16	R.s	10.359	488
17	B.g	7.48	510
18	B.g	18.987	644
19	R.s	10.872	666
20	B.g	16.224	698
21	R.s	10.382	708
22	R.s	12.601	698
23	R.s	9.563	507
24	R.s	7.459	544
25	R.s	8.537	661
26	R.s	8.594	415
27	R.s	10.632	701
28	R.s	14.225	550
29	B.g	7.419	401
30	R.s	9.883	525
31	B.g	12.132	701
32	B.g	7.575	507
33	R.s	12.368	621
34	R.s	7.71	388
35	R.s	7.96	546
36	R.s	10.781	643

37	R.s	10.711	592
38	B.g	9.398	642
39	B.g	7.983	635
40	R.s	10.96	697
41	R.s	12.402	722
42	R.s	10.932	738
43	B.g	9.703	685
44	R.s	7.85	530
45	R.s	11.008	683
46	R.s	7.669	538
47	R.s	12.02	691
48	R.s	7.1	528
49	R.s	5.824	496
50	R.s	10.317	621
51	R.s	8.857	533
52	R.s	10.397	675
53	R.s	8.468	583
54	R.s	9.632	595
55	B.g	13.52	698
56	B.g	4.429	468
57	R.s	12.458	701
58	R.s	10.881	634
59	B.g	13.95	663
60	B.g	9.597	668
61	R.s	10.651	665
62	R.s	7.591	757
63	B.g	11.008	603
64	R.s	11.616	601
65	B.g	13.93	641
66	B.g	12.6	750
67	R.s	12	807
68	B.g	14.5	834
69	R.s	11.912	735
70	R.s	10.416	705
71	B.g	9.808	741
72	R.s	11.802	798
73	B.g	11.902	781
74	B.g	8.762	727
75	R.s	9.281	694
76	R.s	11.686	760

Appendix 2 The location of HOBO water level loggers

Sample plots	**Latitude**	**Longitude**
Plot 1	24.485631	124.229893
Plot 2	24.485355	124.228902
Plot 3	24.485095	124.229286
Plot 4	24.485011	124.229894
Plot 5	24.483529	124.231357
Plot 6	24.484409	124.231423
Plot 7	24.484520	124.231951
Plot 8	24.485679	124.232821
Plot 9	24.484225	124.231764

Appendix 3 The environmental setting for deep learning with PyTorch on Window system